

Similarity Contrastive Estimation for Image and Video Soft Contrastive Self-Supervised Learning

Julien Denize^{1,2*}, Jaonary Rabarisoa^{1†}, Astrid Orcesi^{1†} and Romain Hérault^{2†}

¹LVA, CEA LIST, Université Paris-Saclay, Palaiseau, F-91120, France.

²LITIS, INSA Rouen, Normandie Univ, Saint Etienne du Rouvray, 76801, France.

*Corresponding author. E-mail: julien.denize@cea.fr;

Contributing authors: jaonary.rabarisoa@cea.fr; astrid.orcesi@cea.fr;
romain.herault@insa-rouen.fr;

†These authors contributed equally to this work.

Abstract

Contrastive representation learning has proven to be an effective self-supervised learning method for images and videos. Most successful approaches are based on Noise Contrastive Estimation (NCE) and use different views of an instance as positives that should be contrasted with other instances, called negatives, that are considered as noise. However, several instances in a dataset are drawn from the same distribution and share underlying semantic information. A good data representation should contain relations between the instances, or semantic similarity and dissimilarity, that contrastive learning harms by considering all negatives as noise. To circumvent this issue, we propose a novel formulation of contrastive learning using semantic similarity between instances called Similarity Contrastive Estimation (SCE). Our training objective is a soft contrastive one that brings the positives closer and estimates a continuous distribution to push or pull negative instances based on their learned similarities. We validate empirically our approach on both image and video representation learning. We show that SCE performs competitively with the state of the art on the ImageNet linear evaluation protocol for fewer pretraining epochs and that it generalizes to several downstream image tasks. We also show that SCE reaches state-of-the-art results for pretraining video representation and that the learned representation can generalize to video downstream tasks.

Keywords: Self-Supervised learning, Contrastive, Representation

1 Introduction

Self-Supervised learning (SSL) is an unsupervised learning procedure in which the data provides its own supervision to learn a practical representation of the data. A pretext task is designed to make this supervision. The pretrained model is then fine-tuned on downstream tasks and several works have shown that a self-supervised pretrained network can outperform its supervised counterpart

for image (Caron et al, 2020; Grill et al, 2020; Caron et al, 2021) and video (Feichtenhofer et al, 2021; Duan et al, 2022). It has been successfully applied to various image and video applications such as image classification, action classification, object detection and action localization.

Contrastive learning is a state-of-the-art self-supervised paradigm based on Noise Contrastive Estimation (NCE) (Gutmann and Hyvärinen,

2010) whose most successful applications rely on instance discrimination (He et al, 2020; Chen et al, 2020a; Yang et al, 2020; Han et al, 2020a). Pairs of views from same images or videos are generated by carefully designed data augmentations (Chen et al, 2020a; Tian et al, 2020b; Feichtenhofer et al, 2021). Elements from the same pairs are called *positives* and their representations are pulled together to learn view invariant features. Other instances called *negatives* are considered as noise and their representations are pushed away from positives. Frameworks based on contrastive learning paradigm require a procedure to sample positives and negatives to learn a good data representation. Videos add the time dimension that offers more possibilities than images to generate positives such as sampling different clips as positives (Feichtenhofer et al, 2021; Qian et al, 2021b), using different temporal context (Pan et al, 2021; Recasens et al, 2021; Dave et al, 2022).

A large number of negatives is essential (van den Oord et al, 2018) and various strategies have been proposed to enhance the number of negatives (Chen et al, 2020a; Wu et al, 2018; He et al, 2020; Kalantidis et al, 2020). Sampling hard negatives (Kalantidis et al, 2020; Robinson et al, 2021; Wu et al, 2021; Hu et al, 2021b; Dwibedi et al, 2021) improve the representations but can be harmful if they are semantically false negatives which causes the “class collision problem” (Cai et al, 2020; Wei et al, 2021; Chuang et al, 2020).

Other approaches that learn from positive views without negatives have been proposed by predicting pseudo-classes of different views (Caron et al, 2020, 2021; Toering et al, 2022), minimizing the feature distance of positives (Grill et al, 2020; Chen and He, 2021; Feichtenhofer et al, 2021) or matching the similarity distribution between views and other instances (Zheng et al, 2021b). These methods free the mentioned problem of sampling hard negatives.

Based on the weakness of contrastive learning using negatives, we introduce a self-supervised soft contrastive learning approach called Similarity Contrastive Estimation (SCE), that contrasts positive pairs with other instances and leverages the push of negatives using the inter-instance similarities. Our method computes relations defined as a sharpened similarity distribution between augmented views of a batch. Each view from the batch is paired with a differently augmented

query. Our objective function will maintain for each query the relations and contrast its positive with other images or videos. A memory buffer is maintained to produce a meaningful distribution. Experiments on several datasets show that our approach outperforms our contrastive and relational baselines MoCov2 (Chen et al, 2020c) and ReSSL (Zheng et al, 2021b) on images. We also demonstrate using relations for video representation learning is better than contrastive learning.

Our contributions can be summarized as follows:

- We propose a self-supervised soft contrastive learning approach called Similarity Contrastive Estimation (SCE) that contrasts pairs of augmented instances with other instances and maintains relations among instances for either image or video representation learning.
- We demonstrate that SCE outperforms on several benchmarks its baselines MoCov2 (Chen et al, 2020c) and ReSSL (Zheng et al, 2021b) on images on the same architecture.
- We show that our proposed SCE is competitive with the state of the art on the ImageNet linear evaluation protocol and generalizes to several image downstream tasks.
- We show that our proposed SCE reaches state-of-the-art results for video representation learning by pretraining on the Kinetics400 dataset as we beat or match previous top-1 accuracy for finetuning on HMDB51 and UCF101 for ResNet3D-18 and ResNet3D-50. We also demonstrate it generalizes to several video downstream tasks.

2 Related Work

2.1 Image Self-Supervised Learning

Early Self-Supervised Learning. In early works, different *pretext tasks* to perform Self-Supervised Learning have been proposed to learn a good data representation. They consist in transforming the input data or part of it to perform supervision such as: instance discrimination (Dosovitskiy et al, 2016), patch localization (Doersch et al, 2015), colorization (Zhang et al, 2016), jigsaw puzzle (Noroozi and Favaro, 2016), counting (Noroozi et al, 2017), angle rotation prediction (Gidaris et al, 2018).

Contrastive Learning. Contrastive learning is a learning paradigm (van den Oord et al, 2018; Wu et al, 2018; Hjelm et al, 2019; Tian et al, 2020a; He et al, 2020; Chen et al, 2020a; Misra and van der Maaten, 2020; Tian et al, 2020b; Caron et al, 2020; Grill et al, 2020; Dwibedi et al, 2021; Hu et al, 2021b; Wang et al, 2021) that outperformed previously mentioned *pretext tasks*. Most successful methods rely on instance discrimination with a *positive* pair of views from the same image contrasted with all other instances called *negatives*. Retrieving lots of negatives is necessary for contrastive learning (van den Oord et al, 2018) and various strategies have been proposed. MoCo(v2) (He et al, 2020; Chen et al, 2020c) uses a small batch size and keeps a high number of negatives by maintaining a memory buffer of representations via a momentum encoder. Alternatively, SimCLR (Chen et al, 2020a,b) and MoCov3 (Chen et al, 2021b) use a large batch size without a memory buffer, and without a momentum encoder for SimCLR.

Sampler for Contrastive Learning. All negatives are not equal (Cai et al, 2020) and hard negatives, negatives that are difficult to distinguish with positives, are the most important to sample to improve contrastive learning. However, they are potentially harmful to the training because of the “class collision” problem (Cai et al, 2020; Wei et al, 2021; Chuang et al, 2020). Several samplers have been proposed to alleviate this problem such as using the nearest neighbor as positive for NNCLR (Dwibedi et al, 2021). Truncated-triplet (Wang et al, 2021) optimizes a triplet loss using the k-th similar element as negative that showed significant improvement. It is also possible to generate views by adversarial learning as AdCo (Hu et al, 2021b) showed.

Contrastive Learning without negatives. Various siamese frameworks perform contrastive learning without the use of negatives to avoid the class collision problem. BYOL (Grill et al, 2020) trains an online encoder to predict the output of a momentum updated target encoder. SwAV (Caron et al, 2020) enforces consistency between online cluster assignments from learned prototypes. DINO (Caron et al, 2021) proposes a self-distillation paradigm to match distribution on pseudo class from an online encoder to a momentum target encoder. Barlow-Twins (Zbontar et al,

2021) aligns the cross-correlation matrix between two paired outputs to the identity matrix that VICReg (Bardes et al, 2022) stabilizes by adding an intra-batch decorrelation loss function.

Regularized Contrastive Learning. Several works regularize contrastive learning by optimizing a contrastive objective along with an objective that considers the similarities among instances. CO2 (Wei et al, 2021) adds a consistency regularization term that matches the distribution of similarity for a query and its positive. PCL (Li et al, 2021) and WCL (Zheng et al, 2021a) combines unsupervised clustering with contrastive learning to tighten representations of similar instances.

Relational Learning. Contrastive learning implicitly learns relations among instances by optimizing alignment and matching a prior distribution (Wang and Isola, 2020; Chen and Li, 2020). ReSSL (Zheng et al, 2021b) introduces an explicit relational learning objective by maintaining consistency of pairwise similarities between strong and weak augmented views. The pairs of views are not directly aligned which harms the discriminative performance.

In our work, we optimize a contrastive learning objective using negatives that alleviate class collision by pulling related instances. We do not use a regularization term but directly optimize a soft contrastive learning objective that leverages the contrastive and relational aspects.

2.2 Video Self-Supervised Learning

Video Self-Supervised Learning follows the advances of Image Self-Supervised Learning and often picked ideas from the image modality with adjustment and improvement to make it relevant for videos and make best use of it.

Pretext tasks. As for images, in early works several *pretext tasks* have been proposed on videos. Some were directly picked from images such as rotation (Jing and Tian, 2018), solving Jigsaw puzzles (Kim et al, 2019) but others have been designed specifically for videos. These specific pretext-tasks include predicting motion and appearance (Wang et al, 2019), the shuffling of frame (Lee et al, 2017; Misra et al, 2016) or clip (Xu et al, 2019; Jenni et al, 2020) order, predicting the speed of the video (Benaim et al, 2020; Yao et al, 2020). These methods have been replaced

over time by more performing approaches that are less limited by a specific pretext task to learn a good representation. Recently, TransRank (Duan et al, 2022) introduced a new paradigm to perform temporal and spatial pretext tasks prediction on a clip relatively to other transformations to the same clip and showed promising results.

Contrastive Learning. Video Contrastive Learning (Han et al, 2020a; Lorre et al, 2020; Yang et al, 2020; Pan et al, 2021; Qian et al, 2021b,a; Feichtenhofer et al, 2021; Recasens et al, 2021; Sun et al, 2021; Dave et al, 2022) has been widely studied in the recent years as it gained interest after its better performance than standard pretext tasks in images. Several works studied how to form positive views from different clips (Han et al, 2020a; Qian et al, 2021b; Feichtenhofer et al, 2021; Pan et al, 2021) to directly apply contrastive methods from images. CVRL (Qian et al, 2021b) extended SimCLR to videos and propose a temporal sampler for creating temporally overlapped but not identical positive views which can avoid spatial redundancy. Also, Feichtenhofer et al (2021) extended SimCLR, MoCo, SwaV and BYOL to videos and studied the effect of using random sampled clips from a video to form views. They pushed further the study to sample several positives to generalize the Multi-crop procedure introduced for images by Caron et al (2020). Some works focused on combining contrastive learning and predicting a pretext task (Piergiovanni et al, 2020; Wang et al, 2020; Chen et al, 2021a; Hu et al, 2021b; Huang et al, 2021; Jenni and Jin, 2021). To help better represent the time dimension, several approaches were designed to use different temporal context width (Pan et al, 2021; Recasens et al, 2021; Dave et al, 2022) for the different views.

Multi-modal Learning. To improve self-supervised representation learning, several approaches made use of several modalities to better capture the spatio-temporal information provided by a video. It can be from text (Sun et al, 2019; Miech et al, 2020), audio (Alwassel et al, 2020; Piergiovanni et al, 2020; Recasens et al, 2021), and optical flow (Han et al, 2020a; Lorre et al, 2020; Han et al, 2020b; Piergiovanni et al, 2020; Hu et al, 2021a; Recasens et al, 2021; Toering et al, 2022).

In our work, we propose a soft contrastive learning objective using only RGB frames that directly generalizes our approach from image with

minor changes. To the best of our knowledge, we are the first to introduce the concept of soft contrastive learning using relations for video self-supervised representation learning.

3 Methodology

In this section, we will introduce our baselines: MoCov2 (Chen et al, 2020c) for the contrastive aspect and ReSSL (Zheng et al, 2021b) for the relational aspect. We will then present our self-supervised soft contrastive learning approach called Similarity Contrastive Estimation (SCE). All these methods share the same architecture illustrated in Fig. 1a. We provide the pseudo-code of our algorithm in Appendix A.

3.1 Contrastive and Relational Learning

Consider $\mathbf{x} = \{\mathbf{x}_k\}_{k \in \{1, \dots, N\}}$ a batch of N images. Siamese momentum methods based on Contrastive and Relational learning, such as MoCo (He et al, 2020) and ReSSL (Zheng et al, 2021b) respectively, produce two views of \mathbf{x} , $\mathbf{x}^1 = t^1(\mathbf{x})$ and $\mathbf{x}^2 = t^2(\mathbf{x})$, from two data augmentation distributions T^1 and T^2 with $t^1 \sim T^1$ and $t^2 \sim T^2$. For ReSSL, T^2 is a weak data augmentation distribution compared to T^1 to maintain relations. \mathbf{x}^1 passes through an online network f_s followed by a projector g_s to compute $\mathbf{z}^1 = g_s(f_s(\mathbf{x}^1))$. A parallel target branch containing a projector g_t and an encoder f_t computes $\mathbf{z}^2 = g_t(f_t(\mathbf{x}^2))$. \mathbf{z}^1 and \mathbf{z}^2 are both l_2 -normalized.

The online branch parameters θ_s are updated by gradient (∇) descent to minimize a loss function \mathcal{L} . The target branch parameters θ_t are updated at each iteration by exponential moving average of the online branch parameters with the *momentum value* m , also called *keep rate*, to control the update such as:

$$\theta_s \leftarrow \text{optimizer}(\theta_s, \nabla_{\theta_s} \mathcal{L}), \quad (1)$$

$$\theta_t \leftarrow m\theta_t + (1 - m)\theta_s. \quad (2)$$

MoCo uses the InfoNCE loss, a similarity based function scaled by the temperature τ that maximizes agreement between the positive pair and push negatives away:

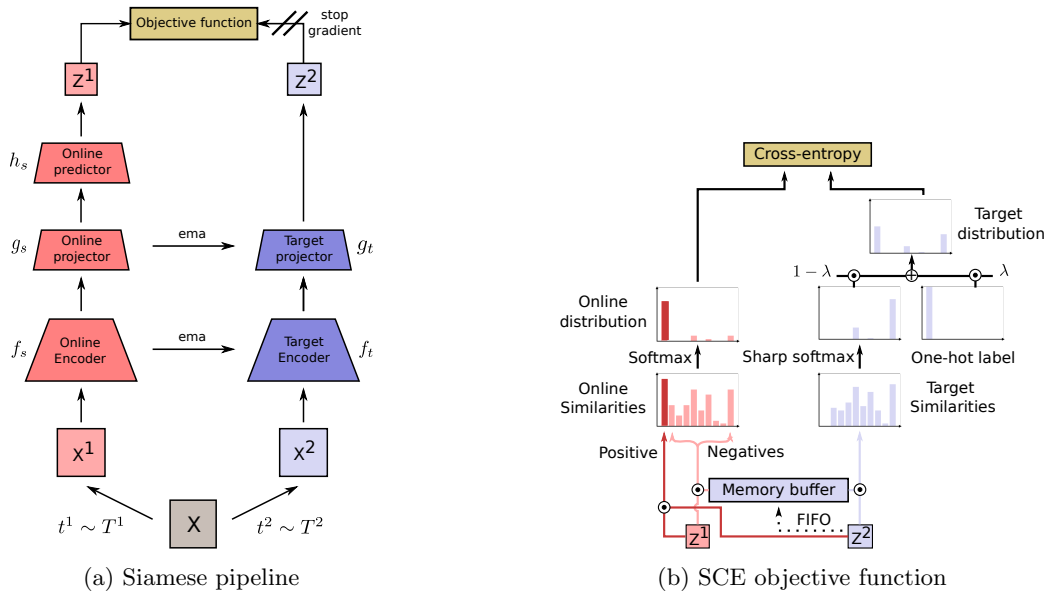


Fig. 1: SCE follows a siamese pipeline illustrated in Fig. 1a. A batch \mathbf{x} of images is augmented with two different data augmentation distributions T^1 and T^2 to form $\mathbf{x}^1 = t^1(\mathbf{x})$ and $\mathbf{x}^2 = t^2(\mathbf{x})$ with $t^1 \sim T^1$ and $t^2 \sim T^2$. The representation \mathbf{z}^1 is computed through an online encoder f_s , projector g_s and optionally a predictor h_s such as $\mathbf{z}^1 = h_s(g_s(f_s(\mathbf{x}^1)))$. A parallel target branch, or ema, computes $\mathbf{z}^2 = g_t(f_t(\mathbf{x}^2))$ with f_t and g_t the target encoder and projector. In the objective function of SCE illustrated in Fig. 1b, \mathbf{z}^2 is used to compute the inter-instance target distribution by applying a sharp softmax to the cosine similarities between \mathbf{z}^2 and a memory buffer of representations from the momentum branch. This distribution is mixed via a $1 - \lambda$ factor with a one-hot label factor λ to form the target distribution. Similarities between \mathbf{z}^1 and the memory buffer plus its positive in \mathbf{z}^2 are also computed. The online distribution is computed via softmax applied to the online similarities. The objective function is the cross entropy between the target and the online distributions.

$$L_{InfoNCE} = -\frac{1}{N} \sum_{i=1}^N \log \left(\frac{\exp(\mathbf{z}_i^1 \cdot \mathbf{z}_i^2 / \tau)}{\sum_{j=1}^N \exp(\mathbf{z}_i^1 \cdot \mathbf{z}_j^2 / \tau)} \right). \quad (3)$$

ReSSL computes a target similarity distribution \mathbf{s}^2 , that represents the relations between weak augmented instances, and the distribution of similarity \mathbf{s}^1 between the strongly augmented instances with the weak augmented ones. Temperature parameters are applied to each distribution: τ for \mathbf{s}^1 and τ_m for \mathbf{s}^2 with $\tau > \tau_m$ to eliminate noisy relations. The loss function is the cross-entropy between \mathbf{s}^2 and \mathbf{s}^1 :

$$s_{ik}^1 = \frac{\mathbb{1}_{i \neq k} \cdot \exp(\mathbf{z}_i^1 \cdot \mathbf{z}_k^2 / \tau)}{\sum_{j=1}^N \mathbb{1}_{i \neq j} \cdot \exp(\mathbf{z}_i^1 \cdot \mathbf{z}_j^2 / \tau)}, \quad (4)$$

$$s_{ik}^2 = \frac{\mathbb{1}_{i \neq k} \cdot \exp(\mathbf{z}_i^2 \cdot \mathbf{z}_k^2 / \tau_m)}{\sum_{j=1}^N \mathbb{1}_{i \neq j} \cdot \exp(\mathbf{z}_i^2 \cdot \mathbf{z}_j^2 / \tau_m)}, \quad (5)$$

$$L_{ReSSL} = -\frac{1}{N} \sum_{i=1}^N \sum_{\substack{k=1 \\ k \neq i}}^N s_{ik}^2 \log(s_{ik}^1). \quad (6)$$

A memory buffer of size $M \gg N$ filled by \mathbf{z}^2 is maintained for both methods.

3.2 Similarity Contrastive Estimation

Contrastive Learning methods damage relations among instances which Relational Learning correctly build. However Relational Learning lacks

the discriminating features that contrastive methods can learn. If we take the example of a dataset composed of cats and dogs, we want our model to be able to understand that two different cats share the same appearance but we also want our model to learn to distinguish details specific to each cat. Based on these requirements, we propose our approach called Similarity Contrastive Estimation (SCE).

We argue that there exists a true distribution of similarity \mathbf{w}_i^* between a query \mathbf{q}_i and the instances in a batch of N images $\mathbf{x} = \{\mathbf{x}_k\}_{k \in \{1, \dots, N\}}$, with \mathbf{x}_i a positive view of \mathbf{q}_i . If we had access to \mathbf{w}_i^* , our training framework would estimate the similarity distribution \mathbf{p}_i between \mathbf{q}_i and all instances in \mathbf{x} , and minimize the cross-entropy between \mathbf{w}_i^* and \mathbf{p}_i which is a soft contrastive learning objective:

$$L_{SCE^*} = -\frac{1}{N} \sum_{i=1}^N \sum_{k=1}^N w_{ik}^* \log(p_{ik}). \quad (7)$$

L_{SCE^*} is a soft contrastive approach that generalizes InfoNCE and ReSSL objectives. InfoNCE is a hard contrastive loss that estimates \mathbf{w}_i^* with a one-hot label and ReSSL estimates \mathbf{w}_i^* without the contrastive component.

We propose an estimation of \mathbf{w}_i^* based on contrastive and relational learning. We consider $\mathbf{x}^1 = t^1(\mathbf{x})$ and $\mathbf{x}^2 = t^2(\mathbf{x})$ generated from \mathbf{x} using two data augmentations $t^1 \sim T^1$ and $t^2 \sim T^2$. Both augmentation distributions should be different to estimate different relations for each view as shown in Sec. 4.1.1. We compute $\mathbf{z}^1 = h_s(g_s(f_s(\mathbf{x}^1)))$ from the online encoder f_s , projector g_s and optionally a predictor h_s (Grill et al, 2020; Chen et al, 2021b). We also compute $\mathbf{z}^2 = g_t(f_t(\mathbf{x}^2))$ from the target encoder f_t and projector g_t . \mathbf{z}^1 and \mathbf{z}^2 are both l_2 -normalized.

The similarity distribution \mathbf{s}_i^2 that defines relations between the query and other instances is computed via the Eq. (5). The temperature τ_m sharpens the distribution to only keep relevant relations. A weighted positive one-hot label is added to \mathbf{s}_i^2 to build the target similarity distribution \mathbf{w}_i^2 :

$$w_{ik}^2 = \lambda \cdot \mathbb{1}_{i=k} + (1 - \lambda) \cdot s_{ik}^2. \quad (8)$$

The online similarity distribution \mathbf{p}_i^1 between \mathbf{z}_i^1 and \mathbf{z}^2 , including the target positive representation in opposition with ReSSL, is computed and scaled by the temperature τ with $\tau > \tau_m$ to build a sharper target distribution:

$$p_{ik}^1 = \frac{\exp(\mathbf{z}_i^1 \cdot \mathbf{z}_k^2 / \tau)}{\sum_{j=1}^N \exp(\mathbf{z}_i^1 \cdot \mathbf{z}_j^2 / \tau)}. \quad (9)$$

The objective function illustrated in Fig. 1b is the cross-entropy between each \mathbf{w}^2 and \mathbf{p}^1 :

$$L_{SCE} = -\frac{1}{N} \sum_{i=1}^N \sum_{k=1}^N w_{ik}^2 \log(p_{ik}^1). \quad (10)$$

The loss can be symmetrized by passing \mathbf{x}^1 and \mathbf{x}^2 through the momentum and online encoders and averaging the two losses computed.

A memory buffer of size $M \gg N$ filled by \mathbf{z}^2 is maintained to better approximate the similarity distributions.

The following proposition explicitly shows that SCE optimizes a contrastive learning objective while maintaining inter-instance relations:

Proposition 1. L_{SCE} defined in Eq. (10) can be written as:

$$L_{SCE} = \lambda \cdot L_{InfoNCE} + \mu \cdot L_{ReSSL} + \eta \cdot L_{Ceil}, \quad (11)$$

with $\mu = \eta = 1 - \lambda$ and

$$L_{Ceil} = -\frac{1}{N} \sum_{i=1}^N \log \left(\frac{\sum_{j=1}^N \mathbb{1}_{i \neq j} \cdot \exp(\mathbf{z}_i^1 \cdot \mathbf{z}_j^2 / \tau)}{\sum_{j=1}^N \exp(\mathbf{z}_i^1 \cdot \mathbf{z}_j^2 / \tau)} \right).$$

The proof separates the positive term and negatives. It can be found in Appendix B. L_{Ceil} leverages how similar the positives should be with hard negatives. Because our approach is a soft contrastive learning objective, we optimize the formulation in Eq. (10) and have the constraint $\mu = \eta = 1 - \lambda$. It frees our implementation from having three losses to optimize with two hyperparameters μ and η to tune. Still, we performed a small study of the objective defined in Eq. (11) without this constraint to check if L_{Ceil} improves results in Sec. 4.1.1.

Parameter	<i>weak</i>	<i>strong</i>	<i>strong-α</i>	<i>strong-β</i>	<i>strong-γ</i>
Random crop probability	1	1	1	1	1
Flip probability	0.5	0.5	0.5	0.5	0.5
Color jittering probability	0.	0.8	0.8	0.8	0.8
Brightness adjustment max intensity	-	0.4	0.4	0.4	0.4
Contrast adjustment max intensity	-	0.4	0.4	0.4	0.4
Saturation adjustment max intensity	-	0.4	0.2	0.2	0.2
Hue adjustment max intensity	-	0.1	0.1	0.1	0.1
Color dropping probability	0.	0.2	0.2	0.2	0.2
Gaussian blurring probability	0.	0.5	1.	0.1	0.5
Solarization probability	0.	0.	0.	0.2	0.2

Table 1: Different distributions of data augmentations applied to SCE. The *weak* distribution is the same as ReSSL (Zheng et al, 2021b), *strong* is the standard contrastive data augmentation (Chen et al, 2020a). The *strong- α* and *strong- β* are two distributions introduced by BYOL (Grill et al, 2020). Finally, *strong- γ* is a mix between *strong- α* and *strong- β* .

λ	0.	0.1	0.2	0.3	0.4	0.5	0.6	0.7	0.8	0.9	1.0
Top-1	81.5	81.8	82.5	82.8	82.9	82.9	82.2	81.6	81.8	81.8	81.1

Table 2: Effect of varying λ on the Top-1 accuracy on ImageNet100. The optimal λ is in [0.4, 0.5] confirming that learning to discriminate and maintaining relations is best.

4 Empirical study

In this section, we will empirically prove the relevance of our proposed Similarity Contrastive Estimation (SCE) self-supervised learning approach to learn a good data representation for both images and videos representation learning.

4.1 Image study

In this section, we first make an ablative study of our approach SCE to find the best hyperparameters on images. Secondly, we compare SCE with its baselines MoCov2 (Chen et al, 2020c) and ReSSL (Zheng et al, 2021b) for the same architecture. Finally, we evaluate SCE on the ImageNet Linear evaluation protocol and assess its generalization capacity on various tasks.

4.1.1 Ablation study

To make the ablation study, we conducted experiments on ImageNet100 that has a close distribution to ImageNet, studied in Sec. 4.1.3, with the advantage to require less resources to train. We keep implementation details close to ReSSL (Zheng et al, 2021b) and MoCov2 (Chen et al, 2020c) to ensure fair comparison.

Dataset. ImageNet (Deng et al, 2009) is a large dataset with 1k classes, almost 1.3M images in the training set and 50K images in the validation set. ImageNet100 is a selection of 100 classes from ImageNet whose classes have been selected randomly. We took the selected classes from (Tian et al, 2020a) referenced in Appendix C.

Implementation details for pretraining. We use the ResNet-50 (He et al, 2016) encoder and pretrain for 200 epochs. We apply by default *strong* and *weak* data augmentations defined in Tab. 1. We do not use a predictor and we do not symmetry the loss by default. Specific hyperparameter details can be found in Appendix D.1.

Evaluation protocol. To evaluate our pre-trained encoders, we train a linear classifier following (Chen et al, 2020c; Zheng et al, 2021b) that is detailed in Appendix D.1.

Leveraging contrastive and relational learning. SCE defined in Eq. (8) leverages contrastive and relational learning via the λ coefficient. We studied the effect of varying the λ coefficient on ImageNet100. Temperature parameters are set to $\tau = 0.1$ and $\tau_m = 0.05$. We report the results in Tab. 2. Performance increases with λ from 0 to 0.5 after which it starts decreasing. The

Method	Loss coefficients			Top-1	
	λ	μ	η	$\tau_m = 0.05$	$\tau_m = 0.07$
InfoNCE	1.	0.	0.	81.11	81.11
	0.5	0.5	0.	82.80	82.49
SCE	0.5	0.5	0.5	82.94	83.37
ReSSL	0.	1.	0.	80.79	78.35
	0.	1.	1.	81.53	79.64

Table 3: Effect of loss coefficients in Eq. (11) on the Top-1 accuracy on ImageNet100. L_{Ceil} consistently improves performance that varies given the temperature parameters.

Online aug	Teacher aug	Sym	top-1
<i>strong</i>	<i>weak</i>	no	82.9
<i>strong-γ</i>	<i>weak</i>	no	83.0
<i>weak</i>	<i>strong</i>	no	73.4
<i>strong</i>	<i>strong</i>	no	80.5
<i>strong-α</i>	<i>strong-β</i>	no	80.7
<i>strong</i>	<i>weak</i>	yes	83.7
<i>strong</i>	<i>strong</i>	yes	83.0
<i>strong-α</i>	<i>strong-β</i>	yes	84.2

Table 4: Effect of using different distributions of data augmentations for the two views and of the loss symmetrization on the Top-1 accuracy on ImageNet100. Using a *weak* view for the teacher without symmetry is necessary to obtain good relations. With loss symmetry, asymmetric data augmentations improve the results, with the best obtained using *strong- α* and *strong- β* .

best λ is inside $[0.4, 0.5]$ confirming that balancing the contrastive and relational aspects provides better representation. In next experiments, we keep $\lambda = 0.5$.

We performed a small study of the optimization of Eq. (11) by removing L_{ceil} ($\eta = 0$) to validate the relevance of our approach for $\tau = 0.1$ and $\tau_m \in \{0.05, 0.07\}$. The results are reported in Tab. 3. Adding the term L_{ceil} consistently improves performance, empirically proving that our approach is better than simply adding $L_{InfoNCE}$ and L_{ReSSL} . This performance boost varies with temperature parameters and our best setting improves by +0.9 percentage points (p.p.) in comparison with adding the two losses.

Asymmetric data augmentations to build the similarity distributions. Contrastive learning approaches use strong data augmentations (Chen et al, 2020a) to learn view invariant

$\tau = 0.1$		$\tau = 0.2$	
τ_m	Top-1	τ_m	Top-1
0.03	82.3	0.03	81.3
0.04	82.5	0.04	81.2
0.05	82.9	0.05	81.2
0.06	82.5	0.06	81.2
0.07	83.4	0.07	81.1
0.08	82.7	0.08	80.9
0.09	82.5	0.09	81.2
0.10	82.1	0.10	81.2

Table 5: Effect of varying the temperature parameters τ_m and τ on the Top-1 accuracy on ImageNet100. τ_m is lower than τ to produce a sharper target distribution without noisy relations. SCE does not collapse when $\tau_m \rightarrow \tau$.

features and prevent the model to collapse. However, these strong data augmentations shift the distribution of similarities among instances that SCE uses to approximate w_i^* in Eq. (8). We need to carefully tune the data augmentations to estimate a relevant target similarity distribution. We listed different distributions of data augmentations in Tab. 1. The *weak* and *strong* augmentations are the same as described by ReSSL (Zheng et al, 2021b). *strong- α* and *strong- β* have been proposed by BYOL (Grill et al, 2020). *strong- γ* combines *strong- α* and *strong- β* .

We performed a study in Tab. 4 on which data augmentations are needed to build a proper target distribution for the non-symmetric and symmetric settings. We report the Top-1 accuracy on Imagenet100 when varying the data augmentations applied on the online and target branches of our pipeline. For the non-symmetric setting, SCE requires the target distribution to be built from a *weak* augmentation distribution that maintains consistency across instances.

Once the loss is symmetrized, asymmetry with strong data augmentations has better performance. Indeed, using *strong- α* and *strong- β* augmentations is better than using *weak* and *strong* augmentations, and same *strong* augmentations has lower performance. We argue symmetrized SCE requires asymmetric data augmentations to produce different relations for each view to make the model learn more information. The effect of using stronger augmentations is balanced by averaging the results on both views. Symmetrizing the

Method	ImageNet	ImageNet100	Cifar10	Cifar100	STL10	Tiny-IN
MoCov2 (Chen et al, 2020c)	67.5	-	-	-	-	-
MoCov2 [*]	68.8	80.5	87.6	61.0	86.5	45.9
ReSSL (Zheng et al, 2021b)	69.9	-	90.2	63.8	88.3	46.6
ReSSL [*]	70.2	81.6	90.2	64.0	89.1	49.5
SCE (Ours)	70.5	83.4	90.3	65.5	89.9	51.9

Table 6: Comparison of SCE with its baselines MoCov2 (Chen et al, 2020c) and ReSSL (Zheng et al, 2021b) on the Top-1 Accuracy on various datasets. SCE outperforms on all benchmarks its baselines. [*] denotes our reproduction.

loss boosts the performance as for (Grill et al, 2020; Chen and He, 2021).

Sharpening the similarity distributions.

The temperature parameters sharpen the distributions of similarity exponentially. SCE uses the temperatures τ_m and τ for the target and online similarity distributions with $\tau_m < \tau$ to guide the online encoder with a sharper target distribution. We made a temperature search on ImageNet100 by varying τ in $\{0.1, 0.2\}$ and τ_m in $\{0.03, \dots, 0.10\}$. The results are in Tab. 5. We found the best values $\tau_m = 0.07$ and $\tau = 0.1$ proving SCE needs a sharper target distribution. In Appendix E, this parameter search is done for other datasets used in comparison with our baselines. Unlike ReSSL (Zheng et al, 2021b), SCE does not collapse when $\tau_m \rightarrow \tau$ thanks to the contrastive aspect. Hence, it is less sensitive to the temperature choice.

4.1.2 Comparison with our baselines

We compared on 6 datasets how SCE performs against its baselines. We keep similar implementation details to ReSSL (Zheng et al, 2021b) and MoCov2 (Chen et al, 2020c) for fair comparison.

Small datasets. Cifar10 and Cifar100 (Krizhevsky and Hinton, 2009) have 50K training images, 10K test images, 32×32 resolution and 10-100 classes respectively. **Medium datasets.** STL10 (Coates et al, 2011) has a 96×96 resolution, 10 classes, 100K unlabeled data, 5k labeled training images and 8K test images. Tiny-Imagenet (Abai and Rajmalwar, 2019) is a subset of ImageNet with 64×64 resolution, 200 classes, 100k training images and 10K validation images.

Implementation details. Architecture implementation details can be found in Appendix D.1. For MoCov2, we use $\tau = 0.2$ and for ReSSL

their best τ and τ_m reported (Zheng et al, 2021b). For SCE, we use the best temperature parameters from Sec. 4.1.1 for ImageNet and ImageNet100 and from Appendix E for the other datasets. The same architecture for all methods is used except for MoCov2 on ImageNet that kept the ImageNet100 projector to improve results.

Results are reported in Tab. 6. Our baselines reproduction is validated as results are better than those reported by the authors. SCE outperforms its baselines on all datasets proving that our method is more efficient to learn discriminating features on the pretrained dataset. We observe that our approach outperforms more significantly ReSSL on smaller datasets than ImageNet, suggesting that it is more important to learn to discriminate among instances for these datasets. SCE has promising applications to domains with few data such as in medical applications.

4.1.3 ImageNet Linear Evaluation

We compare SCE on the widely used ImageNet linear evaluation protocol with the state of the art. We scaled our method using a larger batch size and a predictor to match state-of-the-art results (Grill et al, 2020; Chen et al, 2021b).

Implementation details. We use the ResNet-50 (He et al, 2016) encoder, apply *strong- α* and *strong- β* augmentations defined in Tab. 1. We follow the same training hyperparameters used by (Chen et al, 2021b) and detailed in Appendix D.2. The loss is symmetrized and we keep the best hyperparameters from Sec. 4.1.1: $\lambda = 0.5$, $\tau = 0.1$ and $\tau_m = 0.07$.

Multi-crop setting. We follow (Hu et al, 2021b) setting and sample 6 different views detailed in Appendix D.2.

Method	100	200	300	800-1000
SimCLR (Chen et al, 2020a)	66.5	68.3	-	70.4
MoCov2 (Chen and He, 2021)	67.4	69.9	-	72.2
SwaV (Caron et al, 2020)	66.5	69.1	-	71.8
BYOL (Grill et al, 2020)	66.5	70.6	72.5	74.3
Barlow-Twins(Zbontar et al, 2021)	-	-	71.4	73.2
AdCo (Hu et al, 2021b)	-	68.6	-	72.8
ReSSL (Zheng et al, 2021b)	-	71.4	-	-
WCL (Zheng et al, 2021a)	68.1	70.3	-	72.2
VICReg (Bardes et al, 2022)	-	-	-	73.2
UniGrad (Tao et al, 2022)	<u>70.3</u>	-	-	-
MoCov3 (Chen et al, 2021b)	68.9	-	<u>72.8</u>	74.6
NNCLR (Dwibedi et al, 2021)	69.4	70.7	-	75.4
Triplet (Wang et al, 2021)	-	73.8	-	75.9
SCE (Ours)	72.1	<u>72.7</u>	73.3	74.1

Table 7: State-of-the-art results on the Top-1 Accuracy on ImageNet under the linear evaluation protocol at different pretraining epochs: 100, 200, 300, 800+. SCE is Top-1 at 100 epochs and Top-2 for 200 and 300 epochs. For 800+ epochs, SCE has lower performance than several state-of-the-art methods. Results style: **best**, second best.

Method	Epochs	Top-1
UniGrad (Tao et al, 2022)	100	72.3
SwaV (Caron et al, 2020)	200	72.7
AdCo (Hu et al, 2021b)	200	73.2
WCL (Zheng et al, 2021a)	200	73.3
Triplet (Wang et al, 2021)	200	74.1
ReSSL (Zheng et al, 2021b)	200	74.7
WCL (Zheng et al, 2021a)	800	74.7
SwaV (Caron et al, 2020)	800	75.3
DINO (Caron et al, 2021)	800	75.3
UniGrad (Tao et al, 2022)	800	75.5
NNCLR (Dwibedi et al, 2021)	1000	75.6
AdCo (Hu et al, 2021b)	800	75.7
SCE (ours)	200	75.4

Table 8: State-of-the-art results on the Top-1 Accuracy on ImageNet under the linear evaluation protocol with multi-crop. SCE is competitive with the best state-of-the-art methods by pretraining for only 200 epochs instead of 800+.

Evaluation protocol. We follow the protocol defined by (Chen et al, 2021b) and detailed in Appendix D.2.

We evaluated SCE at epochs 100, 200, 300 and 1000 on the Top-1 accuracy on ImageNet to study the efficiency of our approach and compare it with the state of the art in Tab. 7. At 100 epochs,

SCE reaches **72.1%** up to **74.1%** at 1000 epochs. Hence, SCE has a fast convergence and few epochs of training already provides a good representation. SCE is the Top-1 method at 100 epochs and Top-2 for 200 and 300 epochs proving the good quality of its representation for few epochs of pretraining.

At 1000 epochs, SCE is below several state-of-the-art results. We argue that SCE suffers from maintaining a λ coefficient to 0.5 and that relational or contrastive aspects do not have the same impact at the beginning and at the end of pre-training. A potential improvement would be using a scheduler on λ that varies over time.

We added multi-crop to SCE for 200 epochs of pretraining. It enhances the results but it is costly in terms of time and memory. It improves the results from 72.7% to our best result **75.4%** (+**2.7p.p.**). Therefore, SCE learns from having local views and they should maintain relations to learn better representations. We compared SCE with state-of-the-art methods using multi-crop in Tab. 8. SCE is competitive with top state-of-the-art methods that trained for 800+ epochs by having slightly lower accuracy than the best method using multi-crop ($-0.3p.p$) and without multi-crop ($-0.5p.p$). SCE is more efficient than other methods, as it reaches state-of-the-art results for fewer pretraining epochs.

Method	Food	CIFAR10	CIFAR100	SUN	Cars	Air.	VOC	DTD	Pets	Caltech	Flow.	Avg.
SimCLR	72.8	90.5	74.4	60.6	49.3	49.8	81.4	75.7	84.6	89.3	92.6	74.6
BYOL	75.3	91.3	78.4	62.2	67.8	60.6	82.5	75.5	90.4	94.2	96.1	79.5
NNCLR	76.7	93.7	79.0	62.5	67.1	64.1	83.0	75.5	91.8	91.3	95.1	80
SCE (Ours)	77.7	94.8	80.4	65.3	65.7	59.6	84.0	77.1	90.9	92.7	96.1	80.4
Supervised	72.3	93.6	78.3	61.9	66.7	61.0	82.8	74.9	91.5	94.5	94.7	79.3

Table 9: Linear classifier trained on popular many-shot recognition datasets in comparison with SimCLR (Chen et al, 2020a), BYOL (Grill et al, 2020), NNCLR (Dwivedi et al, 2021) and supervised training. SCE is Top-1 on 7 datasets and in average.

Method	K = 16	K = 32	K = 64	full
MoCov2 (Chen et al, 2020c)	76.1	79.2	81.5	84.6
PCLv2 (Li et al, 2021)	78.3	80.7	82.7	85.4
ReSSL (Zheng et al, 2021b)	79.2	82.0	83.8	86.3
SwAV (Caron et al, 2020)	78.4	81.9	84.4	87.5
WCL (Zheng et al, 2021a)	80.2	83.0	85.0	87.8
SCE (Ours)	79.5	83.1	85.5	88.2

Table 10: Transfer learning on low-shot image classification on Pascal VOC2007. All methods have been pretrained for 200 epochs. SCE is Top-1 when using 32-64-all images per class and Top-2 for 16 images.

Method	AP^{Box}	AP^{Mask}
Random	35.6	31.4
Rel-Loc (Doersch et al, 2015)	40.0	35.0
Rot-Pred (Gidaris et al, 2018)	40.0	34.9
NPID (Wu et al, 2018)	39.4	34.5
MoCo (He et al, 2020)	40.9	35.5
MoCov2 (Chen et al, 2020c)	40.9	35.5
SimCLR (Chen et al, 2020a)	39.6	34.6
BYOL (Grill et al, 2020)	40.3	35.1
SCE (Ours)	<u>41.6</u>	<u>36.0</u>
Triplet (Wang et al, 2021)	41.7	36.2
Supervised	40.0	34.7

Table 11: Object detection and Instance Segmentation on COCO (Lin et al, 2014) training a Mask R-CNN (He et al, 2017). SCE is Top-2 on both tasks, slightly below Truncated-Triplet (Wang et al, 2021) and better than supervised training. Results style: **best**, second best.

4.1.4 Transfer Learning

We study the generalization of our proposed SCE on several tasks using our multi-crop checkpoint pretrained for 200 epochs on ImageNet.

Low-shot evaluation. Low-shot transferability of our backbone is evaluated on Pascal VOC2007. We followed the protocol proposed by Zheng et al (2021b). We select 16, 32, 64 or all images per class to train the classifier. Our results are compared with other state-of-the-art methods

pretrained for 200 epochs in Tab. 10. SCE is Top-1 for 32, 64 and all images per class and Top-2 for 16 images per class, proving the generalization of our approach to few-shot learning.

Linear classifier for many-shot recognition datasets. We follow the same protocol as Grill et al (2020); Ericsson et al (2021) to study many-shot recognition in transfer learning on the datasets FGVC Aircraft (Maji et al, 2013), Caltech-101 (Fei-Fei et al, 2007), Stanford Cars (Krause et al, 2013), CIFAR-10 (Krizhevsky and Hinton, 2009), CIFAR-100 (Krizhevsky and Hinton, 2009), DTD (Cimpoi et al, 2014), Oxford 102 Flowers (Nilsback and Zisserman, 2008), Food-101 (Bossard et al, 2014), Oxford-IIIT Pets (Parkhi et al, 2012), SUN397 (Xiao et al, 2010) and Pascal VOC2007 (Everingham et al, 2010). These datasets cover a large variety of number of training images (2k-75k) and number of classes (10-397). We report the Top-1 classification accuracy except for Aircraft, Caltech-101, Pets and Flowers for which we report the mean per-class accuracy and the 11-point MAP for VOC2007.

We report the performance of SCE in comparison with state-of-the-art methods in Tab. 9. SCE outperforms on 7 datasets all approaches. In average, SCE is above all state-of-the-art methods as well as the supervised baseline, meaning SCE is able to generalize to a wide range of datasets.

Object detection and instance segmentation. We performed object detection and instance segmentation on the COCO dataset (Lin et al, 2014). We used the pretrained network to initialize a Mask R-CNN (He et al, 2017) up to the C4 layer. We follow the protocol of Wang et al (2021) and report the Average Precision for detection AP^{Box} and instance segmentation AP^{Mask} .

We report our results in Tab. 11 and observe that SCE is the second best method after Truncated-Triplet (Wang et al, 2021) on both metrics, by being slightly below their reported results and above the supervised setting. Therefore our proposed SCE is able to generalize to object detection and instance segmentation task beyond what the supervised pretraining can (+1.6p.p. of AP^{Box} and +1.3p.p. of AP^{Mask}).

4.2 Video study

In this section, we first make an ablation study of our approach SCE to find the best hyperparameters on videos. Then, we compare SCE to the state of the art after pretraining on Kinetics400 and assess generalization on various tasks.

4.2.1 Ablation study

Pretraining Dataset. To make the ablation study, we perform pretraining experiments on Mini-Kinetics200 (Xie et al, 2018), later called Kinetics200 for simplicity. It is a subset of Kinetics400 (Kay et al, 2017) meaning they have a close distribution with less resources required on Kinetics200 to train. Kinetics400 is composed of 216k videos for training and 18k for validation for 400 action classes. However, it has been created from Youtube and some videos have been deleted. We use the dataset hosted¹ by the CVD foundation.

Evaluation Datasets. To study the quality of our pretrained representation, we perform linear evaluation classification on the Kinetics200 dataset. Also, we finetune on the first split of the UCF101 (Soomro et al, 2012) and HMDB51 (Kuehne et al, 2011) datasets. UCF101 is an action classification dataset that contains 13k3 different videos for 101 classes and has 3 different training and validation splits. HMDB51 is also an action classification dataset that contains 6k7

Method	K200	UCF101	HMDB51
SCE Baseline	63.9	86.3	57.0
Supervised	72.0	87.5	60.1

Table 12: Comparison of our baseline and supervised training on the Kinetics200, UCF101 and HMDB51 Top-1 accuracy. Supervised training is consistently better.

different videos from 51 classes with 3 different splits.

Pretraining implementation details. We used the ResNet3D-18 network (Hara et al, 2018) following the Slow path of Feichtenhofer et al (2019). We kept hyperparameters close to the ones used for ImageNet in Sec. 4.1.3. More details can be found in Appendix D.3. We pretrain for 200 epochs with a batch size of 512. The loss is symmetrized. To form two different views from a video, we follow Feichtenhofer et al (2021) and randomly sample two clips from the video that lasts 2.56 seconds and keep only 8 frames.

Linear evaluation and finetuning evaluation protocols. We follow Feichtenhofer et al (2021) and details can be found in Appendix D.3. For finetuning on UCF101 and HMDB51 we only use the first split in ablation study.

Baseline and supervised learning. We define an SCE baseline which uses the hyperparameters $\lambda = 0.5$, $\tau = 0.1$, $\tau_m = 0.07$. We provide performance of our SCE baseline as well as supervised training in Tab. 12. We observe that our baseline has lower results than supervised learning with -8.1 p.p for Kinetics200, -1.2 p.p for UCF101 and -3.1 p.p for HMDB51 which shows that our representation has a large margin for improvement.

Leveraging contrastive and relational learning. As for the image study, we varied λ from the equation Eq. (8) in the set $\{0, 0.125, \dots, 0.875, 1\}$ to observe the effect of leveraging the relational and contrastive aspects and report results in Sec. 4.2.1. Using relations during pretraining improves the results rather than only optimizing a contrastive learning objective. The performance on Kinetics200, UCF101 and HMDB51 consistently increases by decreasing λ from 1 to 0.25. The best λ obtained is 0.125. Moreover $\lambda = 0$ performs better than $\lambda = 1$. These results suggest that for video pretraining

¹Link to the Kinetics400 dataset hosted by the CVD foundation: <https://github.com/cvdfoundation/kinetics-dataset>.

λ	K200	UCF101	HMDB51
0.000	64.2	86.2	57.5
0.125	64.8	86.9	58.2
0.250	64.3	86.7	58.2
0.375	64.7	86.3	56.8
0.500	63.9	86.3	57.0
0.625	63.4	86.2	55.7
0.750	63.1	85.8	56.2
0.875	62.1	85.7	55.3
1.000	61.9	85.0	55.4

Table 13: Effect of varying λ on the Kinetics200, UCF101 and HMDB51 Top-1 accuracy. The best λ is 0.125 meaning contrastive and relational leverage increases performance.

τ_m	K200	UCF101	HMDB51
0.03	63.4	86.1	56.9
0.04	63.8	86.6	56.6
0.05	64.3	86.4	57.1
0.06	64.1	86.2	56.4
0.07	63.9	86.3	57.0
0.08	63.8	85.9	55.8

Table 14: Effect of varying τ_m on the Top-1 accuracy on Kinetics200, UCF101 and HMDB51 while maintaining $\tau = 0.1$. The best τ_m is 0.05 meaning that a sharper target distribution is required.

with standard image contrastive learning augmentations, relational learning performs better than contrastive learning and leveraging both further improve the quality of the representation.

Target temperature variation. We studied the effect of varying the target temperature with values in the set $\tau_m \in \{0.03, 0.04, \dots, 0.08\}$ while maintaining the online temperature $\tau = 0.1$. We report results in Sec. 4.2.1. We observe that the best temperature is $\tau_m = 0.05$ indicating that a sharper target distribution is required for video pretraining. We also observe that varying τ_m has a lower impact on performance than varying λ .

Spatial and temporal augmentations. We tested varying and adding some data augmentations that generates the pairs of views. As we are dealing with videos, these augmentations can be either spatial or temporal. We define the *jitter* augmentation that jitters by a factor the duration of a clip, *reverse* that randomly reverses the order of frames and *diff* that randomly applies RGB difference on the frames. RGB difference consists in

strength	K200	UCF101	HMDB51
0.50	63.9	86.3	57.0
0.75	64.6	86.8	57.8
1.00	64.8	87.0	58.1

Table 15: Effect of strength for color jittering for *strong- α* and *strong- β* augmentations on the Kinetics200, UCF101 and HMDB51 Top-1 accuracy. Strong color jittering improves performance.

jitter	reverse	diff	K200	UCF101	HMDB51
0.0	0.0	0.0	63.9	86.3	57.0
0.2	0.0	0.0	64.2	86.4	56.9
0.0	0.2	0.0	64.0	85.7	55.4
0.0	0.0	0.2	65.4	88.3	61.4
0.0	0.0	0.5	64.1	87.7	60.8
Supervised			72.0	87.5	60.1

Table 16: Effect of using the temporal augmentations by applying clip duration jittering *jitter*, randomly reversing the order of frames *reverse* or randomly using RGB difference *diff* on the Kinetics200, UCF101 and HMDB51 Top-1 accuracy. The *diff* augmentation consistently improves results on the three benchmarks and outperforms supervised pretraining. The other augmentations unchanged or decrease performance in average.

converting the frames to grayscale and subtracting them over time to approximate the magnitude of optical flow. In this work, we consider RGB difference as a data augmentation that is randomly applied during pretraining. In the literature it is often used as a modality to provide better representation quality than RGB frames (Jing and Tian, 2018; Lorre et al, 2020; Duan et al, 2022). Here, we only apply it during pretraining as a random augmentation. Evaluation only sees RGB frames.

We tested to increase the color jittering strength in Tab. 15. Using a strength of 1.0 improved our performance on all the benchmarks suggesting that video pretraining requires harder spatial augmentations than images.

We tested our defined temporal augmentations with *jitter* of factor 0.2, meaning sampling clips between 0.80×2.56 and 1.20×2.56 seconds, randomly applying *reverse* with 0.2 probability and randomly applying *diff* with 0.2 or 0.5

λ	τ_m	diff	strength	K200	UCF101	HMDB51
0.125	0.05	0.2	1.0	65.0	87.4	<u>61.1</u>
0.125	0.07	0.2	1.0	64.7	88.2	60.6
0.500	0.05	0.2	1.0	<u>66.0</u>	<u>88.4</u>	62.0
0.500	0.07	0.2	1.0	65.4	88.6	61.0
SCE Baseline				63.9	86.3	57.0
Supervised				72.0	87.5	60.1

Table 17: Effect of combining best hyper-parameters found in the ablation study which are $\lambda = 0.125$, $\tau_m = 0.05$, *color strength* = 1.0 and adding randomly time difference on the Kinetics200, UCF101 and HMDB51 Top-1 accuracy. Using time difference and stronger color jittering increases the optimal λ value which indicates contrastive learning is efficient to deal with harder views and helps relational learning. The best value $\tau_m = 0.05$ performs favorably for Kinetics200 and HMDB51. Results style: **best**, second best.

probability. We report results in Tab. 16. Varying the clip duration had no noticeable impact on our benchmarks, but reversing the order of frames decreased the performance on UCF101 and HMDB51. This can be explained by the fact that this augmentation can prevent the model to correctly represent the arrow of time. Finally, applying *diff* with 0.2 probability considerably improved our performance over our baseline with **+1.5p.p.** on Kinetics200, **+2.0p.p.** on UCF101 and **+4.4p.p.** on HMDB51. It outperforms supervised learning for generalization with **+0.8p.p.** on UCF101 and **+1.3p.p.** on HMDB51. Applying more often *diff* decreases performance. These results show that SCE benefits from using views that are more biased towards motion than appearance. We believe that it is particularly efficient to model relations based on motion.

Bringing all together. We studied varying one hyperparameter from our baseline and how it affects performance. In this final study, we combined our baseline with the different best hyperparameters found which are $\lambda = 0.125$, $\tau_m = 0.05$, *color strength* = 1.0 and applying *diff* with 0.2 probability. We report results in Tab. 17 and found out that using harder augmentations increased the optimal λ value as using $\lambda = 0.5$ performs better than $\lambda = 0.125$. This indicates that relational learning by itself cannot learn a better representation through positive views that share less mutual information. The contrastive aspect of our approach is proven efficient for such harder positives. We take as best configuration $\lambda = 0.5$, $\tau_m = 0.05$, *diff* applied with probability 0.2 and *color strength* = 1.0 as it provides best

or second best results for all our benchmarks. It improves our baseline by **+2.1p.p.** on Kinetics200 and UCF101, and **+5.0p.p.** on HMDB51. It outperforms our supervised baseline by **+0.9p.p.** on UCF101 and **+1.9p.p.** on HMDB51.

4.2.2 Comparison with the State of the Art

Pretraining dataset. To compare SCE with the state of the art, we perform pretraining on Kinetics400 (Kay et al, 2017) introduced in Sec. 4.2.1.

Evaluation datasets. UCF101 (Soomro et al, 2012) and HMDB51 (Kuehne et al, 2011) have been introduced in Sec. 4.2.1.

AVA (v2.2) (Gu et al, 2018) is a dataset used for spatiotemporal localization of humans actions composed of 211k training videos and 57k validation videos for 60 different classes. Bounding box annotations are used as targets and we report the mean Average Precision (mAP) for evaluation.

Something-Something V2 (SSv2) (Goyal et al, 2017) is a dataset composed of human-object interactions for 174 different classes. It contains 169k training and 25k validation videos.

Pretraining implementation details. We use the ResNet3D-18 and ResNet3D-50 network (Hara et al, 2018) and more specifically the slow path of Feichtenhofer et al (2019). We kept the best hyperparameters from Sec. 4.2.1 which are $\lambda = 0.5$, $\tau_m = 0.05$, RGB difference with probability of 0.2, and *color strength* = 1.0 on top of the *strong - α* and *strong - β* augmentations. From the randomly sampled clips we specify if we keep 8 or 16 frames.

Method	T_p	Res_p	T_e	Res_e	Modality	Pretrain	K400	UCF101	HMDB51
Backbone: S3D									
CoCLR (Han et al, 2020b)	32	128 ²	32	128 ²	R	K400	-	87.9	54.6
CoCLR (Han et al, 2020b)	32	128 ²	32	128 ²	R+F	K400	-	90.6	62.9
Backbone: S3D-G									
SpeedNet (Benaim et al, 2020)	64	-	16	224 ²	R	K400	-	81.1	48.8
TEC (Jenni and Jin, 2021)	32	128 ²	32	128 ²	R	K400	-	86.9	63.5
ρ BYOL ($\rho = 4$) (Feichtenhofer et al, 2021)	32	224 ²	32	256 ²	R	K400	-	96.3	75.0
Backbone: R(2+1)D-18									
VideoMoCo (Pan et al, 2021)	32	112 ²	-	-	R	K400	-	78.7	49.2
RSPNet (Chen et al, 2021a)	16	112 ²	16	224 ²	R	K400	-	81.1	44.6
TransRank (Duan et al, 2022)	16	112 ²	-	-	R	K200	-	87.8	60.1
TransRank (Duan et al, 2022)	16	112 ²	-	-	R+RD	K200	-	90.7	64.2
TEC (Jenni and Jin, 2021)	16	112 ²	16	112 ²	R	K400	-	88.2	62.2
Backbone: ResNet3D-18									
ST-Puzzle (Kim et al, 2019)	16	-	16	112 ²	R	K400	-	65.8	33.7
3D-RotNet (Jing and Tian, 2018)	16	112 ²	-	-	R	K400	-	66.0	37.1
3D-RotNet (Jing and Tian, 2018)	16	112 ²	-	-	R+D	K400	-	76.7	47.0
VTHCL (Yang et al, 2020)	8	224 ²	8	224 ²	R	K400	-	80.6	48.6
TransRank (Duan et al, 2022)	16	112 ²	-	-	R	K200	-	85.7	58.1
TransRank (Duan et al, 2022)	16	112 ²	-	-	R+RD	UCF101	-	88.5	63.0
TransRank (Duan et al, 2022)	16	112 ²	-	-	R+RD	K200	-	89.6	63.5
TEC (Jenni and Jin, 2021)	16	128 ²	16	128 ²	R	K400	-	87.1	63.6
ProViCo (Park et al, 2022)	16	112 ²	-	-	R	K400	-	87.2	59.4
ρ MoCo ($\rho = 2$) (Feichtenhofer et al, 2021)	8	224 ²	8	256 ²	R	K400	56.2	87.1	-
SCE (Ours)	8	224 ²	8	256 ²	R	K200	-	88.4	62.0
SCE (Ours)	16	112 ²	16	128 ²	R	K400	56.6	89.1	66.6
SCE (Ours)	8	224 ²	8	256 ²	R	K400	59.8	90.9	65.7
Backbone: ResNet3D-50									
VTHCL (Yang et al, 2020)	8	224 ²	8	224 ²	R	K400	-	82.1	49.2
CATE (Sun et al, 2021)	8	224 ²	32	256 ²	R	K400	-	88.4	61.9
CVRL (Qian et al, 2021b)	16	224 ²	32	256 ²	R	K400	66.1	92.2	66.7
CVRL (Qian et al, 2021b)	16	224 ²	32	256 ²	R	K600	70.4	93.4	68.0
CORP _f (Hu et al, 2021a)	16	224 ²	32	256 ²	R+F	K400	66.6	93.5	68.0
ConST-CL (Yuan et al, 2022)	16	224 ²	32	256 ²	R	K400	66.6	94.8	71.9
BraVe (Recasens et al, 2021)	16	224 ²	32	224 ²	R	K400	-	93.7	72.0
BraVe (Recasens et al, 2021)	16	224 ²	32	224 ²	R+F	K400	-	94.7	72.7
BraVe (Recasens et al, 2021)	16	224 ²	32	224 ²	R	K600	-	94.1	74.0
BraVe (Recasens et al, 2021)	16	224 ²	32	224 ²	R+F	K600	-	95.1	74.3
ρ MoCo ($\rho = 2$) (Feichtenhofer et al, 2021)	8	224 ²	8	256 ²	R	K400	65.8	91.0	-
ρ MoCo ($\rho = 2$) (Feichtenhofer et al, 2021)	16	224 ²	16	256 ²	R	K400	67.6	93.3	-
ρ BYOL ($\rho = 2$) (Feichtenhofer et al, 2021)	8	224 ²	8	256 ²	R	K400	65.8	92.7	-
ρ BYOL ($\rho = 4$) (Feichtenhofer et al, 2021)	8	224 ²	8	256 ²	R	K400	70.0	94.2	72.1
ρ BYOL ($\rho = 4$) (Feichtenhofer et al, 2021)	8	224 ²	16	256 ²	R	K400	71.5	95.5	73.6
SCE (Ours)	8	224 ²	8	256 ²	R	K400	67.6	94.1	70.5
SCE (Ours)	16	224 ²	16	256 ²	R	K400	69.6	95.3	74.7

Table 18: Performance of SCE for the linear evaluation protocol on Kinetics400 and finetuning on the three splits of UCF101 and HMDB51. Res_p , Res_e means the resolution for pretraining and evaluation. T_p , T_e means the number of frames used for pretraining and evaluation. For **Modality**, “R” means RGB, “F” means Optical Flow, “RD” means RGB difference. Best viewed in color, gray rows highlight multi-modal trainings and green rows our results. SCE obtains state of the art results on ResNet3D-18 and on the finetuning protocol for ResNet3D-50.

Method	Res _p	T _p	Res _e	T _e	Pretrain	UCF101			HMDB51		
						R@1	R@5	R@10	R@1	R@5	R@10
Backbone: ResNet3D-18											
MemDPC (Han et al, 2020a)	40	224 ²	40	224 ²	UCF101	20.2	40.4	52.4	7.7	25.7	40.6
RSPNet (Chen et al, 2021a)	16	112 ²	16	224 ²	K400	41.1	59.4	68.4	-	-	-
MFO (Qian et al, 2021a)	16	112 ²	16	112 ²	K400	41.5	60.6	71.2	20.7	40.8	55.2
TransRank (Duan et al, 2022)	16	112 ²	-	-	UCF101	46.5	63.7	-	19.4	45.4	59.1
ViCC (Toering et al, 2022)	16	128 ²	16	128 ²	UCF101	50.3	70.9	78.7	22.7	46.2	60.9
TransRank (Duan et al, 2022)	16	112 ²	-	-	K200	54.0	71.8	-	25.5	52.3	65.8
TCLR (Dave et al, 2022)	16	112 ²	-	-	UCF101	56.2	72.2	79.0	22.8	45.4	57.8
TEC (Jenni and Jin, 2021)	16	128 ²	16	128 ²	UCF101	63.6	79.0	84.8	32.2	60.3	71.6
ProViCo (Park et al, 2022)	16	112 ²	-	-	UCF101	63.8	75.1	84.8	35.9	55.2	74.3
ProViCo (Park et al, 2022)	16	112 ²	-	-	K400	67.6	81.4	90.1	40.1	60.6	75.2
SCE (Ours)	16	112 ²	16	128 ²	K400	74.5	85.9	90.5	37.8	62.1	73.8
SCE (Ours)	8	224 ²	8	256 ²	K400	74.4	85.6	90.0	40.1	63.3	75.4
Backbone: ResNet3D-50											
CATE (Sun et al, 2021)	8	224 ²	32	256 ²	K400	54.9	68.3	75.1	33.0	56.8	69.4
SCE (Ours)	8	224 ²	8	256 ²	K400	81.5	89.7	92.8	43.0	67.0	79.0
SCE (Ours)	16	224 ²	16	256 ²	K400	83.9	92.2	94.9	45.9	69.9	80.5

Table 19: Performance of SCE for video retrieval on the first split of UCF101 and HMDB51. **Res_p**, **Res_e** means the resolution for pretraining and evaluation. **T_p**, **T_e** means the number of frames used for pretraining and evaluation. We report the recall R@1, R@5, R@10. We obtain state of the art results for ResNet3D-18 on both benchmarks and further improve our results using the larger network ResNet3D-50.

Action recognition. We compare SCE on the linear evaluation protocol on Kinetics400 and finetuning on UCF101 and HMDB51. We kept the same implementation details as in Sec. 4.2.1. We compare our results with the state of the art in Tab. 18 on various architectures. To propose a fair comparison, we indicate for each approach the pretraining dataset, the number of frames and resolution used during pre-training as well as during evaluation. For the unknown parameters, we leave the cell empty. We compared with some approaches that used the other visual modalities Optical Flow and RGB difference and the different convolutional backbones S3D (Zhang et al, 2018) and R(2+1)D-18 (Tran et al, 2018).

On ResNet3D-18 even when comparing with methods using several modalities, by using 8×224^2 frames we obtain state-of-the-art results on the three benchmarks with **59.8%** accuracy on Kinetics400, **90.9%** on UCF101, **65.7%** on HMDB51. Using 16×112^2 frames, which is commonly used with this network, improved by +0.9p.p on HMDB51 and decreased by -3.2p.p on kinet-ics400 and -1.8 on UCF101 and keep state of the art results on all benchmarks, except on UCF101 with -0.5p.p compared with Duan et al (2022) using RGB and RGB difference modalities.

On ResNet3D-50, we obtain state-of-the-art results using 16×224^2 frames on HMDB51 with **74.7%** accuracy even when comparing with methods using several modalities. On UCF101, with **95.3%** SCE is on par with the state of the art, -0.2p.p. than (Feichtenhofer et al, 2021), but on Kinetics400 -1.9p.p for **69.6%**. We have the same computational budget as they use 4 views for pretraining. Using 8 frames decreased performance by -2.0p.p., -1.2p.p. and -4.2p.p on Kinetics400, UCF101 and HMDB51. It maintains results that outperform on the three benchmarks ρ MoCo and ρ BYOL with 2 views. It suggests that SCE is more efficient with fewer resources than these methods. By comparing our best with approaches on the S3D backbone that better fit smaller datasets, SCE has slightly lower performance than the state of the art: -1.0p.p. on UCF101 and -0.3p.p. on HMDB51.

Video retrieval. We performed video retrieval on our pretrained backbones on the first split of UCF101 and HMDB51. To perform this task, we extract from the training and testing splits the features using the 30-crops procedure as for action recognition, detailed in Appendix D.3. We query for each video in the testing split the N nearest neighbors ($N \in \{1, 5, 10\}$) in the

Method	views	T	Linear protocol	Finetuning accuracy		
			K400	UCF101	AVA (mAP)	SSv2
Supervised	1	8	74.7	94.8	22.2	52.8
ρ SimCLR ($\rho = 3$)	3	8	62.0 (-12.7)	87.9 (-6.9)	17.6 (-4.6)	52.0 (-0.8)
ρ SwAV ($\rho = 3$)	3	8	62.7 (-12.0)	89.4 (-5.4)	18.2 (-4.0)	51.7 (-1.1)
ρ BYOL ($\rho = 3$)	3	8	68.3 (-6.4)	93.8 (-1.0)	23.4 (+1.2)	55.8 (+3.0)
ρ MoCo ($\rho = 3$)	3	8	67.3 (-7.4)	92.8 (-2.0)	20.3 (-1.9)	54.4 (+1.8)
SCE (Ours)	2	8	67.6 (-7.1)	94.1 (-0.7)	20.3 (-1.9)	53.9 (+1.1)
SCE (Ours)	2	16	69.6 (-5.1)	95.5 (+0.7)	21.6 (-0.6)	57.2 (+4.4)

Table 20: Performance of SCE in comparison with Feichtenhofer et al (2021) for linear evaluation on Kinetics400 and finetuning on the first split of UCF101, AVA and SSv2. SCE is on par with ρ MoCo for fewer views. Increasing the number of frames outperforms ρ BYOL on Kinetics400, UCF101 and SSv2.

training split using cosine similarities. We report the recall $R@N$ for the different N in Tab. 19.

We compare our results with the state of the art on ResNet3D-18. Our proposed SCE with 16×112^2 frames is Top-1 on UCF101 with **74.5%**, **85.6%** and **90.5%** for $R@1$, $R@5$ and $R@10$. Using 8×224^2 frames slightly decreases results that are still state of the art. On HMDB51, SCE with 8×224^2 frames outperforms the state of the art with **40.1%**, **63.3%** and **75.4%** for $R@1$, $R@5$ and $R@10$. Using 16×112^2 frames decreased results that are competitive with the previous state of the art approach (Park et al, 2022) for -2.3 p.p., $+1.5$ p.p. and -1.4 p.p. on $R@1$, $R@5$ and $R@10$.

We provide results using the larger architecture ResNet3d-50 which increases our performance on both benchmarks and outperforms the state of the art on all metrics to reach **83.9%**, **92.2%** and **94.9%** for $R@1$, $R@5$ and $R@10$ on UCF101 as well as **45.9%**, **69.9%** and **80.5%** for $R@1$, $R@5$ and $R@10$ on HMDB51. Our soft contrastive learning approach makes our representation learn features that cluster similar instances even for generalization.

Generalization to downstream tasks. We follow the protocol introduced by Feichtenhofer et al (2021) to compare the generalization of our ResNet3d-50 backbone on Kinetics400, UCF101, AVA and SSv2 with ρ SimCLR, ρ SwAV, ρ BYOL, ρ MoCo and supervised learning in Tab. 20. To ensure a fair comparison, we provide the number of views used by each method and the number of frames per view for pretraining and evaluation.

For 2 views and 8 frames, SCE is on par with ρ MoCo with 3 views on Kinetics400, AVA and SSv2 but is worst than ρ BYOL especially on AVA. For UCF101, results are better than ρ MoCo

and on par with ρ BYOL. These results indicate that our approach proves more effective than contrastive learning as it reaches similar results than ρ MoCo using one less view. Using 16 frames, SCE outperforms all approaches, including supervised training, on UCF101 and SSv2 but performs worse on AVA than ρ Byol and supervised training. This study shows that SCE can generalize to various video downstream tasks which is a criteria of a good learned representation.

5 Conclusion

In this paper we introduced a self-supervised soft contrastive learning approach called Similarity Contrastive Estimation (SCE). It contrasts pairs of asymmetrical augmented views with other instances while maintaining relations among instances. SCE leverages contrastive learning and relational learning and improves the performance over optimizing only one aspect. We showed that it is competitive with the state of the art on the linear evaluation protocol on ImageNet, on video representation learning and to generalize to several image and video downstream tasks. We proposed a simple but effective initial estimation of the true distribution of similarity among instances. An interesting perspective would be to propose a finer estimation of this distribution.

Acknowledgments This publication was made possible by the use of the Factory-AI supercomputer, financially supported by the Ile-de-France Regional Council, and the HPC resources of IDRIS under the allocation 2022-AD011013575 made by GENCI.

Declarations The authors have no relevant financial or non-financial interests to disclose.

References

- Abai Z, Rajmalwar N (2019) Densenet models for tiny imagenet classification. arXiv abs/1904.10429
- Alwassel H, Mahajan D, Korbar B, et al (2020) Self-supervised learning by cross-modal audio-video clustering. In: *Advances in Neural Information Processing Systems 33: Annual Conference on Neural Information Processing Systems*
- Bardes A, Ponce J, LeCun Y (2022) VICReg: Variance-invariance-covariance regularization for self-supervised learning. In: *International Conference on Learning Representations*
- Benaïm S, Ephrat A, Lang O, et al (2020) Speednet: Learning the speediness in videos. In: *Conference on Computer Vision and Pattern Recognition*, pp 9919–9928, <https://doi.org/10.1109/CVPR42600.2020.00994>
- Bossard L, Guillaumin M, Gool LV (2014) Food-101 - mining discriminative components with random forests. In: *13th European Conference on Computer Vision*, pp 446–461, https://doi.org/10.1007/978-3-319-10599-4_29
- Cai TT, Frankle J, Schwab DJ, et al (2020) Are all negatives created equal in contrastive instance discrimination? arXiv abs/2010.06682
- Caron M, Misra I, Mairal J, et al (2020) Unsupervised learning of visual features by contrasting cluster assignments. In: *Advances in Neural Information Processing Systems 33: Annual Conference on Neural Information Processing Systems*
- Caron M, Touvron H, Misra I, et al (2021) Emerging properties in self-supervised vision transformers. In: *Proceedings of the International Conference on Computer Vision*, pp 6706–6716, <https://doi.org/10.1109/ICCV48922.2021.00951>
- Chen P, Huang D, He D, et al (2021a) Rspnet: Relative speed perception for unsupervised video representation learning. In: *33rd Conference on Innovative Applications of Artificial Intelligence*, pp 1045–1053
- Chen T, Li L (2020) Intriguing properties of contrastive losses. arXiv abs/2011.02803
- Chen T, Kornblith S, Norouzi M, et al (2020a) A simple framework for contrastive learning of visual representations. In: *Proceedings of the 37th International Conference on Machine Learning*, pp 1597–1607
- Chen T, Kornblith S, Swersky K, et al (2020b) Big self-supervised models are strong semi-supervised learners. In: *Advances in Neural Information Processing Systems 33: Annual Conference on Neural Information Processing Systems*
- Chen X, He K (2021) Exploring simple siamese representation learning. In: *Conference on Computer Vision and Pattern Recognition*, pp 15,750–15,758, <https://doi.org/10.1109/CVPR46437.2021.01549>
- Chen X, Fan H, Girshick RB, et al (2020c) Improved baselines with momentum contrastive learning. arXiv abs/2003.04297
- Chen X, Xie S, He K (2021b) An empirical study of training self-supervised vision transformers. In: *International Conference on Computer Vision*, pp 9620–9629, <https://doi.org/10.1109/ICCV48922.2021.00950>
- Chuang C, Robinson J, Lin Y, et al (2020) Debaised contrastive learning. In: *Advances in Neural Information Processing Systems 33: Annual Conference on Neural Information Processing Systems*
- Cimpoi M, Maji S, Kokkinos I, et al (2014) Describing textures in the wild. In: *Conference on Computer Vision and Pattern Recognition*, pp 3606–3613, <https://doi.org/10.1109/CVPR.2014.461>
- Coates A, Ng AY, Lee H (2011) An analysis of single-layer networks in unsupervised feature learning. In: *Proceedings of the Fourteenth*

- International Conference on Artificial Intelligence and Statistics, pp 215–223
- Dave IR, Gupta R, Rizve MN, et al (2022) TCLR: temporal contrastive learning for video representation. *Computer Vision and Image Understanding* p 103406. <https://doi.org/10.1016/j.cviu.2022.103406>
- Deng J, Dong W, Socher R, et al (2009) Imagenet: A large-scale hierarchical image database. In: *Computer Society Conference on Computer Vision and Pattern Recognition*, pp 248–255, <https://doi.org/10.1109/CVPR.2009.5206848>
- Doersch C, Gupta A, Efros AA (2015) Unsupervised visual representation learning by context prediction. In: *International Conference on Computer Vision*, pp 1422–1430, <https://doi.org/10.1109/ICCV.2015.167>
- Dosovitskiy A, Fischer P, Springenberg JT, et al (2016) Discriminative unsupervised feature learning with exemplar convolutional neural networks. *Transactions on Pattern Analysis and Machine Intelligence* pp 1734–1747. <https://doi.org/10.1109/TPAMI.2015.2496141>
- Duan H, Zhao N, Chen K, et al (2022) Transrank: Self-supervised video representation learning via ranking-based transformation recognition. In: *Conference on Computer Vision and Pattern Recognition*, pp 2990–3000, <https://doi.org/10.1109/CVPR52688.2022.00301>
- Dwivedi D, Aytar Y, Tompson J, et al (2021) With a little help from my friends: Nearest-neighbor contrastive learning of visual representations. In: *2021 International Conference on Computer Vision*, pp 9568–9577, <https://doi.org/10.1109/ICCV48922.2021.00945>
- Ericsson L, Gouk H, Hospedales TM (2021) How well do self-supervised models transfer? In: *Conference on Computer Vision and Pattern Recognition*, pp 5414–5423, <https://doi.org/10.1109/CVPR46437.2021.00537>
- Everingham M, Gool LV, Williams CKI, et al (2010) The pascal visual object classes (VOC) challenge. *International Journal of Computer Vision* pp 303–338. <https://doi.org/10.1007/s11263-009-0275-4>
- Fei-Fei L, Fergus R, Perona P (2007) Learning generative visual models from few training examples: An incremental bayesian approach tested on 101 object categories. *Computer Vision and Image Understanding* pp 59–70. <https://doi.org/10.1016/j.cviu.2005.09.012>
- Feichtenhofer C, Fan H, Malik J, et al (2019) Slowfast networks for video recognition. In: *International Conference on Computer Vision*, pp 6201–6210, <https://doi.org/10.1109/ICCV.2019.00630>
- Feichtenhofer C, Fan H, Xiong B, et al (2021) A large-scale study on unsupervised spatiotemporal representation learning. In: *Conference on Computer Vision and Pattern Recognition*, pp 3299–3309, <https://doi.org/10.1109/CVPR46437.2021.00331>
- Gidaris S, Singh P, Komodakis N (2018) Unsupervised representation learning by predicting image rotations. In: *6th International Conference on Learning Representations*
- Goyal R, Kahou SE, Michalski V, et al (2017) The "something something" video database for learning and evaluating visual common sense. In: *International Conference on Computer Vision*, pp 5843–5851, <https://doi.org/10.1109/ICCV.2017.622>
- Grill J, Strub F, Altché F, et al (2020) Bootstrap your own latent - A new approach to self-supervised learning. In: *Advances in Neural Information Processing Systems 33: Annual Conference on Neural Information Processing Systems*
- Gu C, Sun C, Ross DA, et al (2018) Ava: A video dataset of spatio-temporally localized atomic visual actions. In: *Conference on Computer Vision and Pattern Recognition*, pp 6047–6056, <https://doi.org/10.1109/CVPR.2018.00633>
- Gutmann M, Hyvärinen A (2010) Noise-contrastive estimation: A new estimation principle for unnormalized statistical models.

- In: 13th International Conference on Artificial Intelligence and Statistics, pp 297–304
- Han T, Xie W, Zisserman A (2020a) Memory-augmented dense predictive coding for video representation learning. In: Vedaldi A, Bischof H, Brox T, et al (eds) 16th European Conference on Computer Vision, pp 312–329, https://doi.org/10.1007/978-3-030-58580-8_19
- Han T, Xie W, Zisserman A (2020b) Self-supervised co-training for video representation learning. In: Advances in Neural Information Processing Systems 33: Annual Conference on Neural Information Processing Systems
- Hara K, Kataoka H, Satoh Y (2018) Can spatiotemporal 3d cnns retrace the history of 2d cnns and imagenet? In: Conference on Computer Vision and Pattern Recognition, pp 6546–6555, <https://doi.org/10.1109/CVPR.2018.00685>
- He K, Zhang X, Ren S, et al (2016) Deep residual learning for image recognition. In: Conference on Computer Vision and Pattern Recognition, pp 770–778, <https://doi.org/10.1109/CVPR.2016.90>
- He K, Gkioxari G, Dollár P, et al (2017) Mask r-cnn. In: International Conference on Computer Vision, pp 2980–2988, <https://doi.org/10.1109/ICCV.2017.322>
- He K, Fan H, Wu Y, et al (2020) Momentum contrast for unsupervised visual representation learning. In: Conference on Computer Vision and Pattern Recognition, pp 9726–9735, <https://doi.org/10.1109/CVPR42600.2020.00975>
- Hjelm RD, Fedorov A, Lavoie-Marchildon S, et al (2019) Learning deep representations by mutual information estimation and maximization. In: 7th International Conference on Learning Representations
- Hu K, Shao J, Liu Y, et al (2021a) Contrast and order representations for video self-supervised learning. In: International Conference on Computer Vision, pp 7919–7929, <https://doi.org/10.1109/ICCV48922.2021.00784>
- Hu Q, Wang X, Hu W, et al (2021b) Adco: Adversarial contrast for efficient learning of unsupervised representations from self-trained negative adversaries. In: Conference on Computer Vision and Pattern Recognition, pp 1074–1083
- Huang D, Wu W, Hu W, et al (2021) Ascnet: Self-supervised video representation learning with appearance-speed consistency. In: International Conference on Computer Vision, pp 8076–8085, <https://doi.org/10.1109/ICCV48922.2021.00799>
- Ioffe S, Szegedy C (2015) Batch normalization: Accelerating deep network training by reducing internal covariate shift. In: 32nd International Conference on Machine Learning, pp 448–456, <https://doi.org/10.1109/CVPR46437.2021.00113>
- Jenni S, Jin H (2021) Time-equivariant contrastive video representation learning. In: International Conference on Computer Vision, <https://doi.org/10.1109/ICCV48922.2021.00982>
- Jenni S, Meishvili G, Favaro P (2020) Video representation learning by recognizing temporal transformations. In: 16th European Conference on Computer Vision, pp 425–442, https://doi.org/10.1007/978-3-030-58604-1_26
- Jing L, Tian Y (2018) Self-supervised spatiotemporal feature learning via video rotation prediction. arXiv abs/1811.11387
- Kalantidis Y, Saryildiz MB, Pion N, et al (2020) Hard negative mixing for contrastive learning. In: Advances in Neural Information Processing Systems 33: Annual Conference on Neural Information Processing Systems
- Kay W, Carreira J, Simonyan K, et al (2017) The kinetics human action video dataset. arXiv abs/1705.06950
- Kim D, Cho D, Kweon IS (2019) Self-supervised video representation learning with space-time cubic puzzles. In: 31st Innovative Applications of Artificial Intelligence Conference, pp 8545–8552, <https://doi.org/10.1609/aaai.v33i01.33018545>

- Krause J, Stark M, Deng J, et al (2013) 3d object representations for fine-grained categorization. In: International Conference on Computer Vision Workshops, pp 554–561
- Krizhevsky A, Hinton G (2009) Learning multiple layers of features from tiny images.(2009). CsTorontoEdu pp 1–58
- Kuehne H, Jhuang H, Garrote E, et al (2011) HMDB: A large video database for human motion recognition. In: International Conference on Computer Vision, pp 2556–2563, <https://doi.org/10.1109/ICCV.2011.6126543>
- Lee H, Huang J, Singh M, et al (2017) Unsupervised representation learning by sorting sequences. In: International Conference on Computer Vision, pp 667–676, <https://doi.org/10.1109/ICCV.2017.79>
- Li J, Zhou P, Xiong C, et al (2021) Prototypical contrastive learning of unsupervised representations. In: 9th International Conference on Learning Representations
- Lin T, Maire M, Belongie SJ, et al (2014) Microsoft COCO: common objects in context. In: 13th European Conference on Computer Vision, pp 740–755, https://doi.org/10.1007/978-3-319-10602-1_48
- Lorre G, Rabarisoa J, Orcesi A, et al (2020) Temporal contrastive pretraining for video action recognition. In: Winter Conference on Applications of Computer Vision, pp 651–659, <https://doi.org/10.1109/WACV45572.2020.9093278>
- Loshchilov I, Hutter F (2017) SGDR: Stochastic gradient descent with warm restarts. 5th International Conference on Learning Representations <https://arxiv.org/abs/1608.03983>
- Maji S, Rahtu E, Kannala J, et al (2013) Fine-grained visual classification of aircraft. arXiv abs/1306.5151
- Miech A, Alayrac J, Smaira L, et al (2020) End-to-end learning of visual representations from uncurated instructional videos. In: Conference on Computer Vision and Pattern Recognition, pp 9876–9886, <https://doi.org/10.1109/CVPR42600.2020.00990>
- Misra I, van der Maaten L (2020) Self-supervised learning of pretext-invariant representations. In: Conference on Computer Vision and Pattern Recognition, pp 6706–6716, <https://doi.org/10.1109/CVPR42600.2020.00674>
- Misra I, Zitnick CL, Hebert M (2016) Shuffle and learn: Unsupervised learning using temporal order verification. In: 14th European Conference on Computer Vision, pp 527–544, https://doi.org/10.1007/978-3-319-46448-0_32
- Nilsback M, Zisserman A (2008) Automated flower classification over a large number of classes. In: Sixth Indian Conference on Computer Vision, Graphics & Image Processing, pp 722–729, <https://doi.org/10.1109/ICVGIP.2008.47>
- Noroozi M, Favaro P (2016) Unsupervised learning of visual representations by solving jigsaw puzzles. In: 14th European Conference on Computer Vision, pp 69–84, https://doi.org/10.1007/978-3-319-46466-4_5
- Noroozi M, Pirsaviash H, Favaro P (2017) Representation learning by learning to count. In: International Conference on Computer Vision, pp 5899–5907, <https://doi.org/10.1109/ICCV.2017.628>
- van den Oord A, Li Y, Vinyals O (2018) Representation learning with contrastive predictive coding. arXiv abs/1807.03748
- Pan T, Song Y, Yang T, et al (2021) Videomoco: Contrastive video representation learning with temporally adversarial examples. In: Conference on Computer Vision and Pattern Recognition, pp 11,205–11,214, <https://doi.org/10.1109/CVPR46437.2021.01105>
- Park J, Lee J, Kim I, et al (2022) Probabilistic representations for video contrastive learning. In: Conference on Computer Vision and Pattern Recognition, pp 14,691–14,701, <https://doi.org/10.1109/CVPR52688.2022.01430>

- Parkhi OM, Vedaldi A, Zisserman A, et al (2012) Cats and dogs. In: Conference on Computer Vision and Pattern Recognition, pp 3498–3505, <https://doi.org/10.1109/CVPR.2012.6248092>
- Piergiovanni AJ, Angelova A, Ryo MS (2020) Evolving losses for unsupervised video representation learning. In: Conference on Computer Vision and Pattern Recognition, pp 130–139, <https://doi.org/10.1109/CVPR42600.2020.00021>
- Qian R, Li Y, Liu H, et al (2021a) Enhancing self-supervised video representation learning via multi-level feature optimization. In: International Conference on Computer Vision, pp 7970–7981, <https://doi.org/10.1109/ICCV48922.2021.00789>
- Qian R, Meng T, Gong B, et al (2021b) Spatiotemporal contrastive video representation learning. In: Conference on Computer Vision and Pattern Recognition, pp 6964–6974, <https://doi.org/10.1109/CVPR46437.2021.00689>
- Recasens A, Luc P, Alayrac J, et al (2021) Broaden your views for self-supervised video learning. In: International Conference on Computer Vision, pp 1235–1245, <https://doi.org/10.1109/ICCV48922.2021.00129>
- Robinson JD, Chuang C, Sra S, et al (2021) Contrastive learning with hard negative samples. In: 9th International Conference on Learning Representations
- Soomro K, Zamir AR, Shah M (2012) UCF101: A dataset of 101 human actions classes from videos in the wild. arXiv abs/1212.0402
- Sun C, Baradel F, Murphy K, et al (2019) Learning video representations using contrastive bidirectional transformer. arXiv abs/1906.05743
- Sun C, Nagrani A, Tian Y, et al (2021) Composable augmentation encoding for video representation learning. In: International Conference on Computer Vision, pp 8814–8824, <https://doi.org/10.1109/ICCV48922.2021.00871>
- Sutskever I, Martens J, Dahl GE, et al (2013) On the importance of initialization and momentum in deep learning. In: Proceedings of the 30th International Conference on Machine Learning, pp 1139–1147
- Tao C, Wang H, Zhu X, et al (2022) Exploring the equivalence of siamese self-supervised learning via A unified gradient framework. Conference on Computer Vision and Pattern Recognition <https://doi.org/10.1109/CVPR52688.2022.01403>
- Tian Y, Krishnan D, Isola P (2020a) Contrastive multiview coding. In: 16th European Conference on Computer Vision, pp 776–794, https://doi.org/10.1007/978-3-030-58621-8_45
- Tian Y, Sun C, Poole B, et al (2020b) What makes for good views for contrastive learning? In: Advances in Neural Information Processing Systems 33: Annual Conference on Neural Information Processing Systems
- Toering M, Gatopoulos I, Stol M, et al (2022) Self-supervised video representation learning with cross-stream prototypical contrasting. In: Winter Conference on Applications of Computer Vision, pp 846–856, <https://doi.org/10.1109/WACV51458.2022.00092>
- Tran D, Wang H, Torresani L, et al (2018) A closer look at spatiotemporal convolutions for action recognition. In: Conference on Computer Vision and Pattern Recognition, pp 6450–6459, <https://doi.org/10.1109/CVPR.2018.00675>
- Wang G, Wang K, Wang G, et al (2021) Solving inefficiency of self-supervised representation learning. In: International Conference on Computer Vision, pp 9485–9495, <https://doi.org/10.1109/ICCV48922.2021.00937>
- Wang J, Jiao J, Bao L, et al (2019) Self-supervised spatio-temporal representation learning for videos by predicting motion and appearance statistics. In: Conference on Computer Vision and Pattern Recognition, pp 4006–4015, <https://doi.org/10.1109/CVPR.2019.00413>

- Wang J, Jiao J, Liu Y (2020) Self-supervised video representation learning by pace prediction. In: 16th European Conference on Computer Vision, pp 504–521, https://doi.org/10.1007/978-3-030-58520-4_30
- Wang T, Isola P (2020) Understanding contrastive representation learning through alignment and uniformity on the hypersphere. In: Proceedings of the 37th International Conference on Machine Learning, pp 9929–9939
- Wei C, Wang H, Shen W, et al (2021) CO2: consistent contrast for unsupervised visual representation learning. In: 9th International Conference on Learning Representations
- Wu M, Mosse M, Zhuang C, et al (2021) Conditional negative sampling for contrastive learning of visual representations. In: 9th International Conference on Learning Representations
- Wu Z, Xiong Y, Yu SX, et al (2018) Unsupervised feature learning via non-parametric instance discrimination. In: Conference on Computer Vision and Pattern Recognition, pp 3733–3742, <https://doi.org/10.1109/CVPR.2018.00393>
- Xiao J, Hays J, Ehinger KA, et al (2010) SUN database: Large-scale scene recognition from abbey to zoo. In: Conference on Computer Vision and Pattern Recognition, pp 3485–3492, <https://doi.org/10.1109/CVPR.2010.5539970>
- Xie S, Sun C, Huang J, et al (2018) Rethinking spatiotemporal feature learning: Speed-accuracy trade-offs in video classification. In: 15th European Conference on Computer Vision, pp 318–335, https://doi.org/10.1007/978-3-030-01267-0_19
- Xu D, Xiao J, Zhao Z, et al (2019) Self-supervised spatiotemporal learning via video clip order prediction. In: Conference on Computer Vision and Pattern Recognition, pp 10,334–10,343, <https://doi.org/10.1109/CVPR.2019.01058>
- Yang C, Xu Y, Dai B, et al (2020) Video representation learning with visual tempo consistency. arXiv abs/2006.15489
- Yao Y, Liu C, Luo D, et al (2020) Video playback rate perception for self-supervised spatio-temporal representation learning. In: Conference on Computer Vision and Pattern Recognition, pp 6547–6556, <https://doi.org/10.1109/CVPR42600.2020.00658>
- You Y, Gitman I, Ginsburg B (2017) Large batch training of convolutional networks. arXiv abs/1708.03888
- Yuan L, Qian R, Cui Y, et al (2022) Contextualized spatio-temporal contrastive learning with self-supervision. In: Conference on Computer Vision and Pattern Recognition, pp 13,957–13,966, <https://doi.org/10.1109/CVPR52688.2022.01359>
- Zbontar J, Jing L, Misra I, et al (2021) Barlow twins: Self-supervised learning via redundancy reduction. In: 38th International Conference on Machine Learning, pp 12,310–12,320
- Zhang D, Dai X, Wang X, et al (2018) S3D: single shot multi-span detector via fully 3d convolutional networks. In: British Machine Vision Conference, p 293
- Zhang R, Isola P, Efros AA (2016) Colorful image colorization. In: 14th European Conference on Computer Vision, pp 649–666, https://doi.org/10.1007/978-3-319-46487-9_40
- Zheng M, Wang F, You S, et al (2021a) Weakly supervised contrastive learning. In: International Conference on Computer Vision, pp 10,022–10,031, <https://doi.org/10.1109/ICCV48922.2021.00989>
- Zheng M, You S, Wang F, et al (2021b) ResSl: Relational self-supervised learning with weak augmentation. In: Advances in Neural Information Processing Systems 34: Annual Conference on Neural Information Processing Systems, pp 2543–2555

A Pseudo-Code of SCE

```

1 # dataloader: loader of batches
2 # bsz: batch size
3 # epochs: number of epochs
4 # T1: weak distribution of data augmentations
5 # T2: strong distribution of data augmentations
6 # f_s, g_s, h_s: online encoder, projector, and optional predictor
7 # f_t, g_t: momentum encoder and projector
8 # queue: memory buffer
9 # tau: online temperature
10 # tau_m: momentum temperature
11 # lambda_: coefficient between contrastive and relational aspects
12 # symmetry_loss: if True, symmetries the loss
13
14 def sce_loss(z1, z2):
15     sim2_pos = zeros(bsz)
16     sim2_neg = einsum("nc,kc->nk", z2, queue)
17     sim2 = cat([sim2_pos, sim2_neg]) / tau_m
18     s2 = softmax(sim2)
19     w2 = lambda_ * one_hot(sim2_pos, bsz+1) + (1 - lambda_) * s
20
21     sim1_pos = einsum("nc,nc->n", z1, z2)
22     sim1_neg = einsum("nc,kc->nk", z1, queue)
23     sim1 = cat([sim1_pos, sim1_neg]) / tau
24     p1 = softmax(sim1)
25
26     loss = cross_entropy(p1, w2)
27     return loss
28
29 for i in range(epochs):
30     for x in dataloader:
31         x1, x2 = T1(x), T2(x)
32
33         z1_s, z2_t = h_s(g_s(f_s(x1))), g_t(f_t(x2))
34         z2_t = stop_grad(z2_t)
35
36         loss = sce_loss(z1_s, z2_t)
37         if symmetry_loss:
38             z1_t, z2_s = g_t(f_t(x1)), h_s(g_s(f_s(x2)))
39             z1_t = stop_grad(z1_t)
40             loss += sce_loss(z2_s, z1_t)
41             loss /= 2
42         loss.backward()
43
44         update(f_s.params)
45         update(g_s.params)
46         update(h_s.params)
47         momentum_update(f_t.params, f_s.params)
48         momentum_update(g_t.params, g_s.params)
49
50         fifo_update(queue, z2_t)
51         if symmetry_loss:
52             fifo_update(queue, z1_t)

```

Algorithm 1: Pseudo-Code of SCE in Pytorch style

B Proof Proposition 1.

Proposition. L_{SCE} defined as

$$L_{SCE} = -\frac{1}{N} \sum_{i=1}^N \sum_{k=1}^N w_{ik}^2 \log(p_{ik}^1),$$

can be written as:

$$L_{SCE} = \lambda \cdot L_{InfoNCE} + \mu \cdot L_{ReSSL} + \eta \cdot L_{Ceil},$$

with $\mu = \eta = 1 - \lambda$ and

$$L_{Ceil} = -\frac{1}{N} \sum_{i=1}^N \log \left(\frac{\sum_{j=1}^N \mathbb{1}_{i \neq j} \cdot \exp(\mathbf{z}_i^1 \cdot \mathbf{z}_j^2 / \tau)}{\sum_{j=1}^N \exp(\mathbf{z}_i^1 \cdot \mathbf{z}_j^2 / \tau)} \right).$$

Proof Recall that:

$$\begin{aligned} p_{ik}^1 &= \frac{\exp(\mathbf{z}_i^1 \cdot \mathbf{z}_k^2 / \tau)}{\sum_{j=1}^N \exp(\mathbf{z}_i^1 \cdot \mathbf{z}_j^2 / \tau)}, \\ s_{ik}^2 &= \frac{\mathbb{1}_{i \neq k} \cdot \exp(\mathbf{z}_i^1 \cdot \mathbf{z}_k^2 / \tau)}{\sum_{j=1}^N \mathbb{1}_{i \neq j} \cdot \exp(\mathbf{z}_i^1 \cdot \mathbf{z}_j^2 / \tau)}, \\ w_{ik}^2 &= \lambda \cdot \mathbb{1}_{i=k} + (1 - \lambda) \cdot s_{ik}^2. \end{aligned}$$

We decompose the second loss over k in the definition of L_{SCE} to make the proof:

$$\begin{aligned} L_{SCE} &= -\frac{1}{N} \sum_{i=1}^N \sum_{k=1}^N w_{ik}^2 \log(p_{ik}^1) \\ &= -\frac{1}{N} \sum_{i=1}^N \left[w_{ii}^2 \log(p_{ii}^1) + \sum_{\substack{k=1 \\ k \neq i}}^N w_{ik}^2 \log(p_{ik}^1) \right] \\ &= \underbrace{-\frac{1}{N} \sum_{i=1}^N w_{ii}^2 \log(p_{ii}^1)}_{(1)} - \underbrace{\frac{1}{N} \sum_{i=1}^N \sum_{\substack{k=1 \\ k \neq i}}^N w_{ik}^2 \log(p_{ik}^1)}_{(2)}. \end{aligned}$$

First we rewrite (1) to retrieve the $L_{InfoNCE}$ loss.

$$\begin{aligned} (1) &= -\frac{1}{N} \sum_{i=1}^N w_{ii}^2 \log(p_{ii}^1) \\ &= -\frac{1}{N} \sum_{i=1}^N \lambda \cdot \log(p_{ii}^1) \\ &= -\lambda \cdot \frac{1}{N} \sum_{i=1}^N \log \left(\frac{\exp(\mathbf{z}_i^1 \cdot \mathbf{z}_i^2 / \tau)}{\sum_{j=1}^N \exp(\mathbf{z}_i^1 \cdot \mathbf{z}_j^2 / \tau)} \right) \\ &= \lambda \cdot L_{InfoNCE}. \end{aligned}$$

Now we rewrite (2) to retrieve the L_{ReSSL} and L_{Ceil} losses.

$$\begin{aligned} (2) &= -\frac{1}{N} \sum_{i=1}^N \sum_{\substack{k=1 \\ k \neq i}}^N w_{ik}^2 \log(p_{ik}^1) \\ &= -\frac{1}{N} \sum_{i=1}^N \sum_{\substack{k=1 \\ k \neq i}}^N (1 - \lambda) \cdot s_{ik}^2 \cdot \log(p_{ik}^1) \\ &= -(1 - \lambda) \cdot \frac{1}{N} \sum_{i=1}^N \sum_{k=1}^N s_{ik}^2 \cdot \log(p_{ik}^1) \\ &= -(1 - \lambda) \cdot \frac{1}{N} \sum_{i=1}^N \sum_{k=1}^N \left[s_{ik}^2 \cdot \log \left(\frac{\exp(\mathbf{z}_i^1 \cdot \mathbf{z}_k^2 / \tau)}{\sum_{j=1}^N \exp(\mathbf{z}_i^1 \cdot \mathbf{z}_j^2 / \tau)} \right) \right] \\ &= -(1 - \lambda) \cdot \frac{1}{N} \sum_{i=1}^N \sum_{k=1}^N \left[s_{ik}^2 \cdot \left(\log \left(\exp(\mathbf{z}_i^1 \cdot \mathbf{z}_k^2 / \tau) \right) - \log \left(\sum_{j=1}^N \exp(\mathbf{z}_i^1 \cdot \mathbf{z}_j^2 / \tau) \right) \right) \right] \\ &= -(1 - \lambda) \cdot \frac{1}{N} \sum_{i=1}^N \sum_{k=1}^N \left[s_{ik}^2 \cdot \left(\log \left(\exp(\mathbf{z}_i^1 \cdot \mathbf{z}_k^2 / \tau) \right) - \log \left(\sum_{j=1}^N \exp(\mathbf{z}_i^1 \cdot \mathbf{z}_j^2 / \tau) \right) + \log \left(\sum_{j=1}^N \mathbb{1}_{i \neq j} \cdot \exp(\mathbf{z}_i^1 \cdot \mathbf{z}_j^2 / \tau) \right) - \log \left(\sum_{j=1}^N \mathbb{1}_{i \neq j} \cdot \exp(\mathbf{z}_i^1 \cdot \mathbf{z}_j^2 / \tau) \right) \right) \right] \\ &= -(1 - \lambda) \cdot \frac{1}{N} \sum_{i=1}^N \sum_{k=1}^N \left[s_{ik}^2 \cdot \left(\log \left(\frac{\exp(\mathbf{z}_i^1 \cdot \mathbf{z}_k^2 / \tau)}{\sum_{j=1}^N \mathbb{1}_{i \neq j} \cdot \exp(\mathbf{z}_i^1 \cdot \mathbf{z}_j^2 / \tau)} \right) + \log \left(\frac{\sum_{j=1}^N \mathbb{1}_{i \neq j} \cdot \exp(\mathbf{z}_i^1 \cdot \mathbf{z}_j^2 / \tau)}{\sum_{j=1}^N \exp(\mathbf{z}_i^1 \cdot \mathbf{z}_j^2 / \tau)} \right) \right) \right] \\ &= -(1 - \lambda) \cdot \frac{1}{N} \left(\sum_{i=1}^N \sum_{k=1}^N \left[s_{ik}^2 \cdot \log \left(\frac{\exp(\mathbf{z}_i^1 \cdot \mathbf{z}_k^2 / \tau)}{\sum_{j=1}^N \mathbb{1}_{i \neq j} \cdot \exp(\mathbf{z}_i^1 \cdot \mathbf{z}_j^2 / \tau)} \right) \right] + \sum_{i=1}^N \sum_{k=1}^N \left[s_{ik}^2 \cdot \log \left(\frac{\sum_{j=1}^N \mathbb{1}_{i \neq j} \cdot \exp(\mathbf{z}_i^1 \cdot \mathbf{z}_j^2 / \tau)}{\sum_{j=1}^N \exp(\mathbf{z}_i^1 \cdot \mathbf{z}_j^2 / \tau)} \right) \right] \right). \end{aligned}$$

Because $s_{ii}^2 = 0$ and \mathbf{s}_i^2 is a probability distribution, we have:

$$\begin{aligned} (2) &= -(1 - \lambda) \cdot \frac{1}{N} \sum_{i=1}^N \sum_{\substack{k=1 \\ k \neq i}}^N \left[s_{ik}^2 \cdot \log \left(\frac{\mathbb{1}_{i \neq k} \cdot \exp(\mathbf{z}_i^1 \cdot \mathbf{z}_k^2 / \tau)}{\sum_{j=1}^N \mathbb{1}_{i \neq j} \cdot \exp(\mathbf{z}_i^1 \cdot \mathbf{z}_j^2 / \tau)} \right) \right] - (1 - \lambda) \cdot \frac{1}{N} \sum_{i=1}^N \left[\log \left(\frac{\sum_{j=1}^N \mathbb{1}_{i \neq j} \cdot \exp(\mathbf{z}_i^1 \cdot \mathbf{z}_j^2 / \tau)}{\sum_{j=1}^N \exp(\mathbf{z}_i^1 \cdot \mathbf{z}_j^2 / \tau)} \right) \right] \\ &= (1 - \lambda) \cdot L_{ReSSL} + (1 - \lambda) \cdot L_{Ceil}. \end{aligned}$$

□

Backbone	Dataset	Projector				Input	Buffer	ema	LR	Batch	WD
		Layers	Hid dim	Out dim	BN						
R-18	CIFAR	2	512	128	hid	32 ²	4,096	0.900	0.06	256	5e ⁻⁴
R-18	STL10	2	512	128	hid	96 ²	16,384	0.996	0.06	256	5e ⁻⁴
R-18	Tiny-IN	2	512	128	hid	64 ²	16,384	0.996	0.06	256	5e ⁻⁴
R-50	IN100	2	4096	256	no	224 ²	65,536	0.996	0.3	512	1e ⁻⁴
R-50	IN1k	3	2048	256	all	224 ²	65,536	0.996	0.5	512	1e ⁻⁴

Table 21: Architecture and hyperparameters used for pretraining on the different datasets. **LR** stands for the initial learning rate, **WD** for weight decay, **BN** for batch normalization (Ioffe and Szegedy, 2015), **Hid** for hidden, **Dim** for dimension, **ema** for the initial momentum value used to update the momentum branch. For **BN**: “no” means no batch normalization is used in the projector, “hid” means batch normalization after each hidden layer, “all” means batch normalization after the hidden layer and the output layer.

C Classes to construct ImageNet100

To build the ImageNet100 dataset, we used the classes shared by the CMC (Tian et al, 2020a) authors in the supplementary material of their publication. We also share these classes in Tab. 22.

100 selected classes from ImageNet			
n02869837	n01749939	n02488291	n02107142
n13037406	n02091831	n04517823	n04589890
n03062245	n01773797	n01735189	n07831146
n07753275	n03085013	n04485082	n02105505
n01983481	n02788148	n03530642	n04435653
n02086910	n02859443	n13040303	n03594734
n02085620	n02099849	n01558993	n04493381
n02109047	n04111531	n02877765	n04429376
n02009229	n01978455	n02106550	n01820546
n01692333	n07714571	n02974003	n02114855
n03785016	n03764736	n03775546	n02087046
n07836838	n04099969	n04592741	n03891251
n02701002	n03379051	n02259212	n07715103
n03947888	n04026417	n02326432	n03637318
n01980166	n02113799	n02086240	n03903868
n02483362	n04127249	n02089973	n03017168
n02093428	n02804414	n02396427	n04418357
n02172182	n01729322	n02113978	n03787032
n02089867	n02119022	n03777754	n04238763
n02231487	n03032252	n02138441	n02104029
n03837869	n03494278	n04136333	n03794056
n03492542	n02018207	n04067472	n03930630
n03584829	n02123045	n04229816	n02100583
n03642806	n04336792	n03259280	n02116738
n02108089	n03424325	n01855672	n02090622

Table 22: The 100 classes selected from ImageNet to construct ImageNet100.

D Implementation details

D.1 Ablation study and baseline comparison for images

Pretraining Implementation details. We use the ResNet-50 (He et al, 2016) encoder for large datasets and ResNet-18 for small and medium datasets with changes detailed below. We pretrain the models for 200 epochs. We apply by default *strong* and *weak* data augmentations, defined in Tab. 1 in the main paper, with the scaling range for the random resized crop set to (0.2, 1.0). Specific hyperparameters for each dataset for the projector construction, the size of the input, the size of the memory buffer, the initial momentum value, the initial learning rate, the batch size and the weight decay applied can be found in Tab. 21. We use the SGD optimizer (Sutskever et al, 2013) with a momentum of 0.9. A linear warmup is applied during 5 epochs to reach the initial learning rate. The learning rate is scaled using the linear scaling rule and follows the cosine decay scheduler without restart (Loshchilov and Hutter, 2017). The momentum value to update the target branch follows a cosine strategy from its initial value to reach 1 at the end of training. We do not symmetrize the loss by default.

Architecture change for small and medium datasets. Because the images are smaller, and ResNet is suitable for larger images, typically 224×224 , we follow guidance from SimCLR (Chen et al, 2020a) and replace the first 7×7 Conv of stride 2 with a 3×3 Conv of stride 1. We also remove the first pooling layer.

Evaluation protocol. To evaluate our pre-trained encoders, we train a linear classifier following (Chen et al, 2020c; Zheng et al, 2021b). We train for 100 epochs on top of the frozen pre-trained encoder using an SGD optimizer with an initial learning rate of 30 without weight decay and a momentum of 0.9. A scheduler is applied to the learning rate that is decayed by a factor of 0.1 at 60 and 80 epochs. The data augmentations for the different datasets are:

- **training set for large datasets:** random resized crop to resolution 224×224 with the scaling range set to (0.08, 1.0) and a random horizontal flip with a probability of 0.5.
- **training set for small and medium datasets:** random resized crop to the dataset resolution with a padding of 4 for small datasets and the scaling range set to (0.08, 1.0). Also, a random horizontal flip with a probability of 0.5 is applied.
- **validation set for large datasets:** resize to resolution 256×256 and center crop to resolution 224×224 .
- **validation set for small and medium datasets:** resize to the dataset resolution.

D.2 Imagenet study

Pretraining implementation details. We use the ResNet-50 (He et al, 2016) encoder and apply *strong- α* and *strong- β* augmentations, defined in Tab. 1 in the main paper, with the scaling range for the random resized crop set to (0.2, 1.0). The batch size is set to 4096 and the memory buffer to 65,536. We follow the same training hyperparameters as (Chen et al, 2021b) for the architecture. Specifically, we use the same projector and predictor, the LARS optimizer (You et al, 2017) with a weight decay of $1.5 \cdot 10^{-6}$ for 1000 epochs of training and 10^{-6} for fewer epochs. Bias and batch normalization (Ioffe and Szegedy, 2015) parameters are excluded. The initial learning rate is 0.5 for 100 epochs and 0.3 for more epochs. It is linearly scaled for 10 epochs and it follows the cosine annealed scheduler. The momentum value follows a cosine scheduler from 0.996 for 1000 epochs, 0.99 for fewer epochs, to reach 1 at the end of training. The loss is symmetrized. For SCE specific hyperparameters, we keep the best from ablation study: $\lambda = 0.5$, $\tau = 0.1$ and $\tau_m = 0.07$.

Multi-crop setting. We follow Hu et al (2021b) and sample 6 different views. The first two views are global views as without multi-crop, meaning resolution of 224×224 and the scaling range for random resized crop set to (0.2, 1.0). The 4 local crops have a resolution of 192×192 , 160×160 , 128×128 , 96×96 and scaling range (0.172, 0.86), (0.143, 0.715), (0.114, 0.571), (0.086, 0.429) on which we apply the *strong- γ* data augmentation defined in Tab. 1 in the main paper.

Evaluation protocol. We follow the protocol defined by (Chen et al, 2021b). Specifically, we train a linear classifier for 90 epochs on top of the frozen encoder with a batch size of 1024 and a SGD optimizer with a momentum of 0.9 and without weight decay. The initial learning rate is 0.1 and scaled using the linear scaling rule and follows the cosine decay scheduler without restart (Loshchilov and Hutter, 2017). The data augmentations applied are:

- **training set:** random resized crop to resolution 224×224 with the scaling range set to (0.08, 1.0) and a random horizontal flip with a probability of 0.5.
- **validation set:** resize to resolution 256×256 and center crop to resolution 224×224 .

D.3 Video study

Pretraining implementation details. We used the ResNet3D-18 and ResNet3D-50 networks (Hara et al, 2018) following the Slow path of Feichtenhofer et al (2019). The exact architecture details can be found in Tab. 23. We kept the siamese architecture used for ImageNet in Sec. 4.1.3 and depending on the backbone and pretraining dataset, the projector and predictor architectures as well as the memory buffer size vary and are referenced in Tab. 24. The LARS optimizer with a weight decay of 1.10^{-6} , batch normalization and bias parameters excluded, for 200 epoch of training is used. The learning rate follows a linear warmup until it reaches an initial value of 2.4 and then follows a cosine annealed scheduler. The initial learning rate is scaled following the linear scaling rule and the batch size is set to 512. The momentum value follows a cosine scheduler from 0.99 to 1 and the loss is symmetrized. To sample and crop different views from a video, we follow Feichtenhofer et al (2021) and sample randomly different clips from the video

stage	ResNet3d-18	ResNet3D-50
conv1	$1 \times 7^2, 64$ stride 1, 2^2	$1 \times 7^2, 64$ stride 1, 2^2
pool1	$1 \times 3^2, max$ stride 1, 2^2	$1 \times 3^2, max$ stride 1, 2^2
res ₂	$\begin{bmatrix} 1 \times 3^2, 64 \\ 1 \times 3^2, 64 \end{bmatrix} \times 2$	$\begin{bmatrix} 1 \times 1^2, 64 \\ 1 \times 3^2, 64 \\ 1 \times 1^2, 256 \end{bmatrix} \times 3$
res ₃	$\begin{bmatrix} 1 \times 3^2, 128 \\ 1 \times 3^2, 128 \end{bmatrix} \times 2$	$\begin{bmatrix} 1 \times 1^2, 128 \\ 1 \times 3^2, 128 \\ 1 \times 1^2, 512 \end{bmatrix} \times 4$
res ₄	$\begin{bmatrix} 3 \times 3^2, 256 \\ 1 \times 3^2, 256 \end{bmatrix} \times 2$	$\begin{bmatrix} 3 \times 1^2, 256 \\ 1 \times 3^2, 256 \\ 1 \times 1^2, 1024 \end{bmatrix} \times 6$
res ₅	$\begin{bmatrix} 3 \times 3^2, 512 \\ 1 \times 3^2, 512 \end{bmatrix} \times 2$	$\begin{bmatrix} 3 \times 1^2, 512 \\ 1 \times 3^2, 512 \\ 1 \times 1^2, 2048 \end{bmatrix} \times 3$
pool	global average	global average

Table 23: ResNet3D-18 and ResNet3D-50 networks.

that lasts 2.56 seconds. For Kinetics it corresponds to 64 frames for a frame rate per second (FPS) of 25. Out of this clip we keep a number of frames specified in the main paper. By default, we sample two different clips to form positives and we apply the *strong- α* and *strong- β* augmentations, defined in Tab. 1 in the main paper, to the views.

Linear evaluation protocol details. We follow Feichtenhofer et al (2021) and train a linear classifier for 60 epochs on top of the frozen encoder with a batch size of 512. We use the SGD optimizer with a momentum of 0.9 and without weight decay to reach the initial learning rate 2 that follows the linear scaling rule with the batch size set to 512. A linear warmup is applied during 35 epochs and then a cosine annealing scheduler. For training, we sample randomly a clip in the video and random crop to the size 224×224 after short scaling the video to 256. An horizontal flip is also applied with a probability of 0.5. For evaluation, we follow the standard evaluation protocol of Feichtenhofer et al (2019) and sample 10 temporal clips with 3 different spatial crops of size 256×256 applied to each temporal clip to cover the whole video. The final

prediction is the mean average of the predictions of the 30 clips sampled.

Finetuning evaluation protocol details.

We follow Feichtenhofer et al (2021) for finetuning on UCF101 and HMDB51. We finetune the whole pretrained network and perform supervised training on the 101 and 51 classes respectively for 200 epochs with dropout of probability 0.8 before classification. We use the SGD optimizer with a momentum of 0.9 and without weight decay to reach the initial learning rate 0.1 that follows the linear scaling rule with the batch size set to 64 and a cosine annealing scheduler without warmup. For training, we sample randomly a clip in the video and random crop to the size 224×224 after short scaling the video to 256. We apply color jittering with the *strong* augmentation parameters, defined in Tab. 1 in the main paper, and an horizontal flip with a probability of 0.5. For evaluation, we follow the 30-crops procedure as for linear evaluation. Specific hyperparameter search for each dataset might improve results.

E Temperature influence on small and medium datasets

We made a temperature search on CIFAR10, CIFAR100, STL10 and Tiny-ImageNet by varying τ in $\{0.1, 0.2\}$ and τ_m in $\{0.03, \dots, 0.10\}$. The results are in Tab. 25. As for ImageNet100, we need a sharper distribution on the output of the momentum encoder. Unlike ReSSL (Zheng et al, 2021b), SCE do not collapse when $\tau_m \rightarrow \tau$ thanks to the contrastive aspect. For our baselines comparison in Sec. 4.2, we use the best temperatures found for each dataset.

Backbone	Dataset	Projector				Predictor				Buffer
		Layers	Hid dim	Out dim	BN	Layers	Hid dim	Out dim	BN	
ResNet3D-18	K200	3	1024	256	all	2	1024	256	hid	32768
ResNet3D-18	K400	3	1024	256	all	2	1024	256	hid	65536
ResNet3D-50	K400	3	4096	256	all	2	4096	256	hid	65536

Table 24: Architecture and hyperparameters used for video pretraining. **BN** stands for for Batch Normalization, **Hid** for hidden, **Dim** for dimension. For **BN**: "hid" means batch normalization after each hidden layer, "all" means batch normalization after the hidden layer and the output layer.

Dataset	τ	$\tau_m = 0.03$	$\tau_m = 0.04$	$\tau_m = 0.05$	$\tau_m = 0.06$	$\tau_m = 0.07$	$\tau_m = 0.08$	$\tau_m = 0.09$	$\tau_m = 0.1$
CIFAR10	0.1	89.93	90.03	90.06	90.20	90.16	90.06	89.67	88.97
CIFAR10	0.2	89.98	90.12	90.12	90.05	90.13	90.09	90.22	90.34
CIFAR100	0.1	64.49	64.90	65.19	65.33	65.27	65.45	64.89	63.87
CIFAR100	0.2	63.71	63.74	63.89	64.05	64.24	64.23	64.10	64.30
STL10	0.1	89.34	89.94	89.87	89.84	89.72	89.52	88.99	88.41
STL10	0.2	88.4	88.23	88.4	88.35	87.54	88.32	88.80	88.59
Tiny-IN	0.1	50.23	51.12	51.41	51.66	51.90	51.58	51.37	50.46
Tiny-IN	0.2	48.56	48.85	48.35	48.98	49.06	49.15	49.66	49.64

Table 25: Effect of varying the temperature parameters τ_m and τ on the Top-1 accuracy.